



Hydroxybenzoic Acid Derivatives as Dual-Target Ligands: Mitochondriotropic Antioxidants and Cholinesterase Inhibitors

Catarina Oliveira¹, Fernando Cagide¹, José Teixeira^{1,2}, Ricardo Amorim^{1,2}, Lisa Sequeira¹, Francesco Mesiti³, Tiago Silva^{1,2}, Jorge Garrido^{1,4}, Fernando Remião⁵, Santiago Vilar⁶, Eugenio Uriarte^{6,7}, Paulo J. Oliveira^{2*} and Fernanda Borges^{1*}

OPEN ACCESS

Edited by:

Stefano Alcaro,
Magna Græcia University, Italy

Reviewed by:

Eugenio Gaudio,
Istituto Oncologico della Svizzera
Italiana, Switzerland
Jose Marco-Contelles,
Consejo Superior de Investigaciones
Científicas (CSIC), Spain
Alfonso T. Garcia-Sosa,
University of Tartu, Estonia

*Correspondence:

Paulo J. Oliveira
pauloliv@cnc.uc.pt
Fernanda Borges
fborges@fc.up.pt

Specialty section:

This article was submitted to
Medicinal and Pharmaceutical
Chemistry,
a section of the journal
Frontiers in Chemistry

Received: 24 February 2018

Accepted: 03 April 2018

Published: 23 April 2018

Citation:

Oliveira C, Cagide F, Teixeira J,
Amorim R, Sequeira L, Mesiti F,
Silva T, Garrido J, Remião F, Vilar S,
Uriarte E, Oliveira PJ and Borges F
(2018) Hydroxybenzoic Acid
Derivatives as Dual-Target Ligands:
Mitochondriotropic Antioxidants and
Cholinesterase Inhibitors.
Front. Chem. 6:126.
doi: 10.3389/fchem.2018.00126

¹ CIQUP, Department of Chemistry and Biochemistry, Faculty of Sciences, University of Porto, Porto, Portugal, ² CNC, Center for Neuroscience and Cell Biology, UC-Biotech, University of Coimbra, Cantanhede, Portugal, ³ Department of "Scienze della Salute", University "Magna Græcia" of Catanzaro, Catanzaro, Italy, ⁴ Department of Chemical Engineering, School of Engineering (ISEP), Polytechnic of Porto, Porto, Portugal, ⁵ UCIBIO-REQUIMTE, Laboratory of Toxicology, Department of Biological Sciences, Faculty of Pharmacy, University of Porto, Porto, Portugal, ⁶ Departamento de Química Orgánica, Facultad de Farmacia, Universidad de Santiago de Compostela, Santiago de Compostela, Spain, ⁷ Instituto de Ciencias Químicas Aplicadas, Facultad de Ingeniería, Universidad Autónoma de Chile, Santiago, Chile

Alzheimer's disease (AD) is a multifactorial age-related disease associated with oxidative stress (OS) and impaired cholinergic transmission. Accordingly, targeting mitochondrial OS and restoring cholinergic transmission can be an effective therapeutic strategy toward AD. Herein, we report for the first time dual-target hydroxybenzoic acid (HBAC) derivatives acting as mitochondriotropic antioxidants and cholinesterase (ChE) inhibitors. The studies were performed with two mitochondriotropic antioxidants **AntiOxBEN₁** (catechol derivative), and **AntiOxBEN₂** (pyrogallol derivative) and compounds **15–18**, which have longer spacers. Compounds **AntiOxBEN₁** and **15**, with a shorter carbon chain spacer (six- and eight-carbon) were shown to be potent antioxidants and BChE inhibitors (IC₅₀ = 85 ± 5 and 106 ± 5 nM, respectively), while compounds **17** and **18** with a 10-carbon chain were more effective AChE inhibitors (IC₅₀ = 7.7 ± 0.4 and 7.2 ± 0.5 μM, respectively). Interestingly, molecular modeling data pointed toward bifunctional ChEs inhibitors. The most promising ChE inhibitors acted by a non-competitive mechanism. In general, with exception of compounds **15** and **17**, no cytotoxic effects were observed in differentiated human neuroblastoma (SH-SY5Y) and human hepatocarcinoma (HepG2) cells, while Aβ-induced cytotoxicity was significantly prevented by the new dual-target HBAC derivatives. Overall, due to its BChE selectivity, favorable toxicological profile, neuroprotective activity and drug-like properties, which suggested blood-brain barrier (BBB) permeability, the mitochondriotropic antioxidant **AntiOxBEN₁** is considered a valid lead candidate for the development of dual acting drugs for AD and other mitochondrial OS-related diseases.

Keywords: hydroxybenzoic acids, oxidative stress, mitochondria-targeted antioxidants, cholinesterase inhibitors, acetyl and butyrylcholinesterase

INTRODUCTION

Alzheimer's disease (AD) is a multifactorial age-related disease, closely associated with impaired cholinergic transmission and oxidative stress (OS), among other factors (Guo et al., 2013; Zheng et al., 2014; Talevi, 2015; Nikolic et al., 2016). According to the cholinergic hypothesis, impairment in the cholinergic function is of critical importance in AD, especially in brain areas like the neocortex and the hippocampus, which control learning, memory, behavior and emotional responses. The levels of acetylcholine (ACh) in the synaptic cleft are tightly regulated by cholinesterases enzymes (ChEs): acetylcholinesterase (AChE) and butyrylcholinesterase (BChE) are the key regulators of cholinergic tone and transmission (Anand and Singh, 2013; Colović et al., 2013). While AChE in the healthy brain predominates, BChE is considered to play a minor role in the regulation of synaptic ACh levels (Li et al., 2017; Shah et al., 2017). However, in advanced stages of AD, AChE activity may decrease approximately by 50% in distinctive regions of the brain while BChE activity is enhanced, making both ChEs stimulating targets for the treatment of AD (Li et al., 2017; Shah et al., 2017). Moreover, it was proposed that low-activity BChE in AD patients correlates with better cognitive function (Holmes et al., 2005). Additionally, it has been shown that ChEs are proteins that colocalize with A β deposits and directly promotes A β assembly and aggregation into insoluble plaques, a classic biochemical hallmark of AD pathology (Morán et al., 1993). These secondary non-cholinergic functions of ChEs are attributed to the peripheral active site (PAS) of the enzyme's active site (Bajda et al., 2013; Silva et al., 2014). While deposition of A β plaques is the hallmark of the disease, the neurotoxicity of A β oligomers was shown to be stronger than that of the fibrils.

Brain is highly vulnerable to OS due to its high-energy demand and oxygen exposure, rich abundance of easily oxidizable polyunsaturated fatty acids, high level of potent reactive oxygen species (ROS), and relative paucity of endogenous antioxidants. OS and mitochondrial damage have been implicated in the pathogenesis of several age-related diseases (Guo et al., 2013). The redox alterations promoted by OS in specific cellular components lead to a more oxidized state, often resulting from an increased production of ROS and/or more limited intrinsic antioxidant activity (Dai et al.,

2014; Dhawan, 2014; Bhat et al., 2015; Ksiazek-Winiarek and Głabinski, 2015). Therefore, it is believed that antioxidant therapy can operate as a pharmacological approach to prevent or delay the OS events that lead to neurodegeneration.

The fact that several drugs exert their effect through the interaction with diverse targets is shifting the drug discovery paradigm from the one target to a multiple-target approach. This approach is becoming increasingly important in drug discovery for multifactorial diseases, such as AD. As such, looking for new chemical entities that can minimize OS and restore cholinergic transmission by targeting ChEs can be a valid pharmacological strategy for the clinical management of AD.

Protocatechuic (PA, **Figure 1**) and gallic acids (GA, **Figure 1**) are hydroxybenzoic acids (HBAC) widely distributed in plants and fruit with diverse biological properties such as antioxidant, anti-inflammatory, antimicrobial and anticancer activity, as well as neuroprotection (Heleno et al., 2015; Pezzini et al., 2017; Sz wajgier et al., 2017). Although this type of dietary antioxidants has promising *in vitro* outcomes, the translation in antioxidant therapy have had a dissatisfying clinical outcome, which has been directly associated with poor bioavailability, particularly inefficient cellular uptake and target selectivity (Guzman-Villanueva et al., 2015). To address this limitation, targeting mitochondria with organelle-specific molecules can be a useful therapeutic strategy for the prevention and/or treatment of OS-related diseases such as AD.

The design and synthesis of two mitochondriotropic antioxidants based on HBAC (**AntiOxBEN₁** and **AntiOxBEN₂**, **Figure 1**), in which PA and GA were covalently bound to a triphenylphosphonium cation (TPP⁺) through a six-carbon aliphatic chain has been previously reported (Teixeira et al., 2017b). AntiOxBENs effectively accumulated in rat liver mitochondria, driven by the negative-inside organelle transmembrane electric potential ($\Delta\Psi$), and prevented lipid peroxidation while exhibiting low toxicity (Teixeira et al., 2017b). AntiOxBENs presented higher lipophilicity than the parent compounds (PA and GA), and similar antioxidant and iron chelating properties.

As part of our drug discovery program, and following an AD multi-target strategy, **AntiOxBEN₁** and **AntiOxBEN₂** were screened in this work toward ChEs. To perform structure-activity relationship studies the series was extended (**Figure 1**) and the antioxidant profile in cell free and cell-based systems as well as the inhibitory activities toward AChE and BChE of the new derivatives were evaluated. The cytotoxicity profile, drug-like properties and mechanism of enzymatic inhibition were also assessed. Moreover, to understand the enzyme(s)-inhibitor(s) interactions, molecular modeling studies were performed using models based in the crystal structures of the targets.

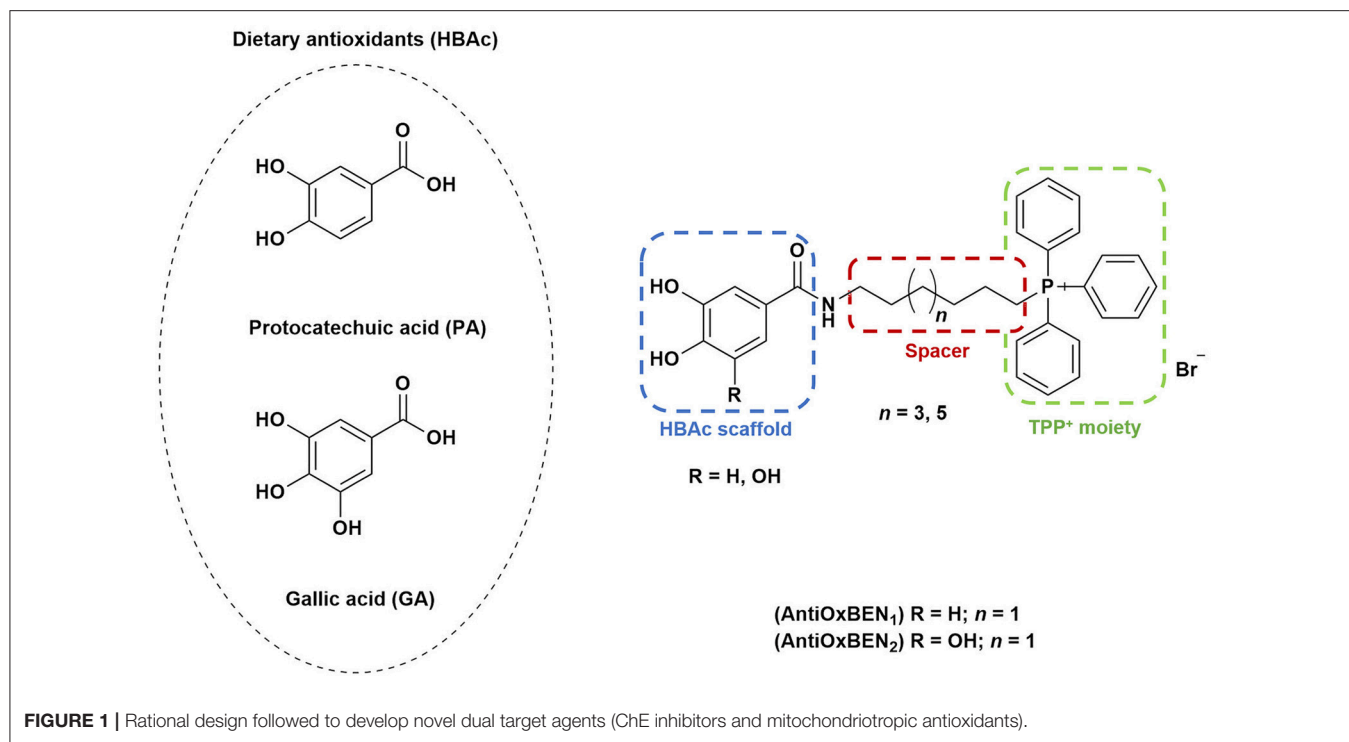
MATERIALS AND METHODS

Chemistry

Reagents and General Conditions

All reagents were purchased from Sigma-Aldrich and TCI Chemicals. All solvents were *pro analysis* grade from Merck, Carlo Erba Reagents and Scharlab.

Abbreviations: ABTS^{•+}, 2,2'-azino-bis(3-ethylbenzthiazoline-6-sulfonic acid); ACh, Acetylcholine; AChE, acetylcholinesterase; AD, Alzheimer's disease; ATCI, Acetylthiocholine iodide; BBB, blood-brain barrier; BCh, butyrylcholine; BChE, butyrylcholinesterase; BTCl, butyrylthiocholine iodide; ChEs, cholinesterases; clogP, logarithm of the octanol-water partition coefficient; CNS, central nervous system; DIPEA, *N,N*-diisopropylethylamine; Diphos, 1,2-bis(diphenylphosphine)ethane; DPPH[•], 2,2'-diphenyl-1-picrylhydrazyl radical; DTNB, 5,5'-dithiobis-(2-nitrobenzoate); EDTA, ethylenediaminetetraacetic acid; FDA, Food and Drug Administration; GA, gallic acid; HBA, number of hydrogen acceptors; HBAC, hydroxybenzoic acid(s); HBD, number of hydrogen donors; HBSS, Hank's balanced salt solution; *K_i*, inhibition constant; *K_m*, Michaelis constant; log BB, blood (plasma)-brain partitioning; NEAA, nonessential amino acids; *n*rotb, number of rotatable bonds; OS, oxidative stress; PA, protocatechuic acid; PPh₃, triphenylphosphine; ROS, reactive oxygen species; TNB²⁻, anion 5-thio-2-nitrobenzoate; TPA, 12-*O*-Tetradecanoylphorbol-13-acetate; TPP⁺, triphenylphosphonium cation; tPSA, topological polar surface area; *V_{max}*, maximum velocity; $\Delta\Psi$, transmembrane electric potential.



Thin layer chromatography (TLC) was performed on precoated silica gel 60 F254 acquired from Merck with layer thickness of 0.2 mm. Reaction control was monitored using ethyl acetate and/or ethyl acetate:methanol (9:1) and spots were visualized under UV detection at 254 and 366 nm. Following the extraction step, the organic layers were dried over anhydrous sodium sulfate. Flash column chromatography was carried out with silica gel 60 0.040–0.063 mm acquired from Carlo-Erba Reactifs. Cellulose flash column chromatography was carried out with cellulose powder 0.01–0.10 mm acquired from Sigma-Aldrich. The elution systems used for flash chromatography were specified for each compound. Solvents were evaporated using a Büchi Rotavapor.

Apparatus

NMR data were acquired on a Bruker Avance III 400 NMR spectrometer, at room temperature, operating at 400.15 MHz for ¹H and 100.62 MHz for ¹³C and DEPT135 (Distortionless Enhancement by Polarization Transfer). Tetramethylsilane (TMS) was used as internal reference; chemical shifts (δ) were expressed in ppm and coupling constants (J) were given in Hz. DEPT135 values were included in ¹³C NMR data (underline values).

Mass spectra (MS) were carried out on a Varian 320-MS (EI) or Bruker Microtof (ESI) apparatus; the data were reported as m/z (% of relative intensity of the most important fragments).

Synthesis of Benzoic Based Derivatives

General procedure used to obtain benzoic acid amide derivatives (3–6).

The appropriate benzoic acid (3,4-dimethoxybenzoic acid (**1**) or 3,4,5-trimethoxybenzoic acid (**2**), 1 mmol) was dissolved in

dichloromethane (15 mL) and POCl₃ (1 mmol) was added at room temperature. After 30 min, the reactional mixture was cooled (ice bath) and 8-aminooctan-1-ol or 10-aminodecan-1-ol (1.2 mmol) and DIPEA (4 mmol) were added. The reaction was stirred for 1–2 h at room temperature. The mixture was extracted with dichloromethane (3 × 20 mL). The organic phases were combined, washed with water, NaHCO₃ 5% (20 mL) and HCl 1 M (20 mL). The organic phases were combined, dried and, after filtration, the solvent was evaporated and the compound purified by silica gel flash chromatography using ethyl acetate as eluting system. The fractions containing the intended compound were collected and the solvent was evaporated to dryness. The reaction was followed by TLC (silica gel, ethyl acetate). The procedure was adapted from the literature (Chen et al., 2013).

N-(8-Hydroxyoctyl)-3,4-dimethoxybenzamide (3). $\eta = 49\%$. ¹H RMN (CDCl₃): $\delta = 1.29$ – 1.38 (8H, *m*, N(CH₂)₂(CH₂)₄), 1.51 – 1.61 (4H, *m*, NCH₂CH₂(CH₂)₄CH₂), 1.63 (1H, *s*, OH), 3.37 – 3.47 (2H, *m*, NCH₂), 3.62 (2H, *t*, $J = 6.6$ Hz, CH₂O), 3.91 (6H, *s*, 2 × OCH₃), 6.19 (1H, *s*, NH), 6.84 (1H, *d*, $J = 8.4$ Hz, H(5)), 7.25 (1H, *dd*, $J = 2.0, 8.4$ Hz, H(6)), 7.41 (1H, *d*, $J = 2.0$ Hz, H(2)). ¹³C RMN (CDCl₃): $\delta = 25.8$ (N(CH₂)₅CH₂), 27.0 (N(CH₂)₂CH₂), 29.3 (N(CH₂)₃CH₂), 29.4 (N(CH₂)₄CH₂), 29.8 (NCH₂CH₂), 32.8 (N(CH₂)₆CH₂), 40.2 (NCH₂), 56.1 (2 × OCH₃), 63.0 (CH₂O), 110.4 (C(5)), 110.8 (C(2)), 119.2 (C(6)), 127.6 (C(1)), 149.1 (C(3)), 151.7 (C(4)), 167.2 (CO). ESI/MS m/z (%): 332 ([M+Na]⁺, 100), 310 ([M+H]⁺, 67), 165 (97).

N-(8-Hydroxyoctyl)-3,4,5-trimethoxybenzamide (4). $\eta = 71\%$. ¹H RMN (CDCl₃): $\delta = 1.28$ – 1.42 (8H, *m*, N(CH₂)₂(CH₂)₄), 1.49 – 1.66 (4H, *m*, NCH₂CH₂(CH₂)₄CH₂), 1.73 (1H, *s*, OH), 3.37 – 3.49 (2H, *m*, NCH₂), 3.62 (2H, *t*, $J = 6.6$ Hz, CH₂O), 3.87 (3H, *s*, OCH₃), 3.89 (6H, *s*, 2 × OCH₃), 6.16 (1H, *s*, NH),

6.98 (2H, s, H(2) and H(6)). ^{13}C RMN (CDCl_3): $\delta = 25.8$ ($\text{N}(\text{CH}_2)_5\text{CH}_2$), 27.0 ($\text{N}(\text{CH}_2)_2\text{CH}_2$), 29.3 ($\text{N}(\text{CH}_2)_3\text{CH}_2$), 29.4 ($\text{N}(\text{CH}_2)_4\text{CH}_2$), 29.8 (NCH_2CH_2), 32.8 ($\text{N}(\text{CH}_2)_6\text{CH}_2$), 40.3 (NCH_2), 56.5 ($2 \times \text{OCH}_3$), 61.0 (OCH_3), 63.1 (CH_2O), 104.5 (C(2) and C(6)), 130.5 (C(1)), 141.0 (C(4)), 153.3 (C(3) and C(5)), 167.4 (CO). ESI/MS m/z (%): 362 ($[\text{M}+\text{Na}]^+$, 57), 340 ($[\text{M}+\text{H}]^+$, 98), 195 (100), 154 (54).

***N*-(10-Hydroxydecyl)-3,4-dimethoxybenzamide (5)**. $\eta = 54\%$. ^1H RMN (CDCl_3): $\delta = 1.24$ – 1.35 (12H, *m*, $\text{N}(\text{CH}_2)_2(\text{CH}_2)_6$), 1.50 – 1.60 (4H, *m*, $\text{NCH}_2\text{CH}_2(\text{CH}_2)_6\text{CH}_2$), 1.61 (1H, *s*, OH), 3.36 – 3.46 (2H, *m*, NCH_2), 3.62 (2H, *t*, $J = 6.6$ Hz, CH_2O), 3.90 (6H, *s*, $2 \times \text{OCH}_3$), 6.17 (1H, *s*, NH), 6.84 (1H, *d*, $J = 8.4$ Hz, H(5)), 7.25 (1H, *dd*, $J = 2.0$, 8.4 Hz, H(6)), 7.41 (1H, *d*, $J = 2.0$ Hz, H(2)). ^{13}C RMN (CDCl_3): $\delta = 25.8$ ($\text{N}(\text{CH}_2)_7\text{CH}_2$), 27.1 ($\text{N}(\text{CH}_2)_2\text{CH}_2$), 29.4 ($\text{N}(\text{CH}_2)_3\text{CH}_2$), 29.5 ($\text{N}(\text{CH}_2)_4\text{CH}_2\text{CH}_2\text{CH}_2$), 29.6 ($\text{N}(\text{CH}_2)_5\text{CH}_2$), 29.8 (NCH_2CH_2), 32.9 ($\text{N}(\text{CH}_2)_8\text{CH}_2$), 40.2 (NCH_2), 56.1 ($2 \times \text{OCH}_3$), 63.1 (CH_2O), 110.4 (C(5)), 110.8 (C(2)), 119.2 (C(6)), 127.7 (C(1)), 149.1 (C(3)), 151.7 (C(4)), 167.2 (CO). ESI/MS m/z (%): 360 ($[\text{M}+\text{Na}]^+$, 43), 338 ($[\text{M}+\text{H}]^+$, 61), 165 (100).

***N*-(10-Hydroxydecyl)-3,4,5-trimethoxybenzamide (6)**. $\eta = 71\%$. ^1H RMN (CDCl_3): $\delta = 1.23$ – 1.36 (12H, *m*, $\text{N}(\text{CH}_2)_2(\text{CH}_2)_6$), 1.49 – 1.62 (4H, *m*, $\text{NCH}_2\text{CH}_2(\text{CH}_2)_6\text{CH}_2$), 1.64 (1H, *s*, OH), 3.36 – 3.49 (2H, *m*, NCH_2), 3.63 (2H, *t*, $J = 6.6$ Hz, CH_2O), 3.86 (3H, *s*, OCH_3), 3.89 (6H, *s*, $2 \times \text{OCH}_3$), 6.11 (1H, *s*, NH), 6.98 (2H, *s*, H(2) and H(6)). ^{13}C RMN (CDCl_3): $\delta = 25.8$ ($\text{N}(\text{CH}_2)_7\text{CH}_2$), 27.1 ($\text{N}(\text{CH}_2)_2\text{CH}_2$), 29.4 ($\text{N}(\text{CH}_2)_3\text{CH}_2$), 29.5 ($\text{N}(\text{CH}_2)_4\text{CH}_2\text{CH}_2\text{CH}_2$), 29.6 ($\text{N}(\text{CH}_2)_5\text{CH}_2$), 29.8 (NCH_2CH_2), 32.9 ($\text{N}(\text{CH}_2)_8\text{CH}_2$), 40.4 (NCH_2), 56.5 ($2 \times \text{OCH}_3$), 61.0 (OCH_3), 63.1 (CH_2O), 104.5 (C(2) and C(6)), 130.5 (C(1)), 141.0 (C(4)), 153.3 (C(3) and C(5)), 167.4 (CO). ESI/MS m/z (%): 368 ($[\text{M}+\text{H}]^+$, 100), 195 (98), 169 (22), 154 (51).

General procedure used to obtain bromo derivatives (7–10)

Benzoic acid amide derivative (3–6) (1 mmol) and 1,2-dibromotetrachloroethane (1 mmol) were dissolved in THF (20 mL). After, 1,2-bis(diphenylphosphine)ethane (diphos) (0.5 mmol) was added and the reaction was stirred at room temperature for 20 h. Then, the reaction mixture was filtered using a Celite pad. After evaporation of the filtrate, an oil residue was obtained. The oil was purified by silica gel flash chromatography using ethyl acetate as eluting system. The fractions containing the intended compound were collected. After the solvent evaporation, the compound was recrystallized from *n*-hexane. The reaction was followed by TLC (silica gel, ethyl acetate). The procedure was adapted from the literature (Pollastri et al., 2001; Teixeira et al., 2017b).

***N*-(8-Bromooctyl)-3,4-dimethoxybenzamide (7)**. $\eta = 64\%$. ^1H RMN (CDCl_3): $\delta = 1.30$ – 1.45 (8H, *m*, $\text{N}(\text{CH}_2)_2(\text{CH}_2)_4$), 1.55 – 1.65 (2H, *m*, NCH_2CH_2), 1.79 – 1.89 (2H, *m*, $\text{N}(\text{CH}_2)_6\text{CH}_2$), 3.39 (2H, *t*, $J = 6.8$ Hz, CH_2Br), 3.40 – 3.45 (2H, *m*, NCH_2), 3.91 (6H, *s*, $2 \times \text{OCH}_3$), 6.12 (1H, *s*, Hz, NH), 6.84 (1H, *d*, $J = 8.4$ Hz, H(5)), 7.25 (1H, *dd*, $J = 2.0$, 8.4 Hz, H(6)), 7.42 (1H, *d*, $J = 2.0$ Hz, H(2)). ^{13}C RMN (CDCl_3): $\delta = 27.0$ ($\text{N}(\text{CH}_2)_2\text{CH}_2$), 28.2 ($\text{N}(\text{CH}_2)_5\text{CH}_2$), 28.8 ($\text{N}(\text{CH}_2)_4\text{CH}_2$), 29.2 ($\text{N}(\text{CH}_2)_3\text{CH}_2$), 29.8 (NCH_2CH_2), 32.9 ($\text{N}(\text{CH}_2)_6\text{CH}_2$), 34.1 (CH_2Br), 40.2 (NCH_2),

56.1 ($2 \times \text{OCH}_3$), 110.4 (C(5)), 110.8 (C(2)), 119.2 (C(6)), 127.7 (C(1)), 149.2 (C(3)), 151.8 (C(4)), 167.2 (CO). ESI/MS m/z (%): 396 ($[\text{M}+\text{Na}+2]^+$, 30), 394 ($[\text{M}+\text{Na}]^+$, 30), 374 ($[\text{M}+\text{H}+2]^+$, 100), 372 ($[\text{M}+\text{H}]^+$, 91), 165 (32), 139 (27), 124 (40).

***N*-(8-Bromooctyl)-3,4,5-trimethoxybenzamide (8)**. $\eta = 69\%$. ^1H RMN (CDCl_3): $\delta = 1.27$ – 1.47 (8H, *m*, $\text{N}(\text{CH}_2)_2(\text{CH}_2)_4$), 1.56 – 1.65 (2H, *m*, NCH_2CH_2), 1.79 – 1.90 (2H, *m*, $\text{N}(\text{CH}_2)_6\text{CH}_2$), 3.40 (2H, *t*, $J = 6.8$ Hz, CH_2Br), 3.41 – 3.47 (2H, *m*, NCH_2), 3.87 (3H, *s*, OCH_3), 3.89 (6H, *s*, $2 \times \text{OCH}_3$), 6.12 (1H, *s*, NH), 6.98 (2H, *s*, H(2) and H(6)). ^{13}C RMN (CDCl_3): $\delta = 27.0$ ($\text{N}(\text{CH}_2)_2\text{CH}_2$), 28.2 ($\text{N}(\text{CH}_2)_5\text{CH}_2$), 28.8 ($\text{N}(\text{CH}_2)_4\text{CH}_2$), 29.2 ($\text{N}(\text{CH}_2)_3\text{CH}_2$), 29.8 (NCH_2CH_2), 32.8 ($\text{N}(\text{CH}_2)_6\text{CH}_2$), 34.1 (CH_2Br), 40.3 (NCH_2), 56.5 ($2 \times \text{OCH}_3$), 61.0 (OCH_3), 104.5 (C(2) and C(6)), 130.4 (C(1)), 141.0 (C(4)), 153.3 (C(3) and C(5)), 167.4 (CO). ESI/MS m/z (%): 426 ($[\text{M}+\text{Na}+2]^+$, 35), 424 ($[\text{M}+\text{Na}]^+$, 39), 404 ($[\text{M}+\text{H}+2]^+$, 78), 402 ($[\text{M}+\text{H}]^+$, 93), 195 (26), 169 (25), 154 (100).

***N*-(10-Bromodecyl)-3,4-dimethoxybenzamide (9)**. $\eta = 62\%$. ^1H RMN (CDCl_3): $\delta = 1.24$ – 1.44 (12H, *m*, $\text{N}(\text{CH}_2)_2(\text{CH}_2)_6$), 1.55 – 1.66 (2H, *m*, NCH_2CH_2), 1.78 – 1.88 (2H, *m*, $\text{N}(\text{CH}_2)_8\text{CH}_2$), 3.39 (2H, *t*, $J = 6.9$ Hz, CH_2Br), 3.41 – 3.46 (2H, *m*, NCH_2), 3.90 (6H, *s*, $2 \times \text{OCH}_3$), 6.83 (1H, *d*, $J = 8.4$ Hz, H(5)), 7.30 (1H, *dd*, $J = 2.0$, 8.4 Hz, H(6)), 7.42 (1H, *d*, $J = 2.0$ Hz, H(2)). ^{13}C RMN (CDCl_3): $\delta = 27.1$ ($\text{N}(\text{CH}_2)_2\text{CH}_2$), 28.2 ($\text{N}(\text{CH}_2)_7\text{CH}_2$), 28.8 ($\text{N}(\text{CH}_2)_6\text{CH}_2$), 29.4 ($\text{N}(\text{CH}_2)_3\text{CH}_2$), 29.5 ($\text{N}(\text{CH}_2)_4(\text{CH}_2)_2$), 29.7 (NCH_2CH_2), 32.9 ($\text{N}(\text{CH}_2)_8\text{CH}_2$), 34.1 (CH_2Br), 40.6 (NCH_2), 56.2 ($2 \times \text{OCH}_3$), 110.4 (C(5)), 110.9 (C(2)), 119.9 (C(6)), 126.3 (C(1)), 149.1 (C(3)), 152.2 (C(4)), 167.9 (CO). ESI/MS m/z (%): 424 ($[\text{M}+\text{Na}+2]^+$, 20), 422 ($[\text{M}+\text{Na}]^+$, 23), 402 ($[\text{M}+\text{H}+2]^+$, 100), 400 ($[\text{M}+\text{H}]^+$, 99), 165 (20), 139 (21), 124 (22).

***N*-(10-Bromodecyl)-3,4,5-trimethoxybenzamide (10)**. $\eta = 63\%$. ^1H RMN (CDCl_3): $\delta = 1.26$ – 1.46 (12H, *m*, $\text{N}(\text{CH}_2)_2(\text{CH}_2)_6$), 1.55 – 1.68 (2H, *m*, NCH_2CH_2), 1.77 – 1.90 (2H, *m*, $\text{N}(\text{CH}_2)_8\text{CH}_2$), 3.40 (2H, *t*, $J = 6.9$ Hz, CH_2Br), 3.40 – 3.48 (2H, *m*, NCH_2), 3.87 (3H, *s*, OCH_3), 3.90 (6H, *s*, $2 \times \text{OCH}_3$), 6.13 (1H, *s*, NH), 6.98 (2H, *s*, H(2) and H(6)). ^{13}C RMN (CDCl_3): $\delta = 27.1$ ($\text{N}(\text{CH}_2)_2\text{CH}_2$), 28.3 ($\text{N}(\text{CH}_2)_7\text{CH}_2$), 28.8 ($\text{N}(\text{CH}_2)_6\text{CH}_2$), 29.4 ($\text{N}(\text{CH}_2)_3\text{CH}_2$), 29.4 ($\text{N}(\text{CH}_2)_4(\text{CH}_2)_2$), 29.8 (NCH_2CH_2), 32.9 ($\text{N}(\text{CH}_2)_8\text{CH}_2$), 34.1 (CH_2Br), 40.4 (NCH_2), 56.5 ($2 \times \text{OCH}_3$), 61.0 (OCH_3), 104.5 (C(2) and C(6)), 130.4 (C(1)), 141.0 (C(4)), 153.3 (C(3) and C(5)), 167.4 (CO). ESI/MS m/z (%): 432 ($[\text{M}+\text{H}+2]^+$, 17), 430 ($[\text{M}+\text{H}]^+$, 13), 195 (23), 169 (25), 154 (100).

General procedure used to obtain triphenylphosphonium salts (11–14)

The appropriate bromo derivative (7–10) (1 mmol) was mixed with triphenylphosphine (PPh_3 , 1 mmol) in a round-bottomed flask and heated to 100°C for 48 h. The residue was purified by silica gel flash chromatography using gradient elution (ethyl acetate:methanol from 9:1 to 6:4). The fractions containing the desired compound were collected and the solvent was evaporated to dryness. The reaction was followed by TLC [silica gel, ethyl acetate:methanol (9:1) and dichloromethane:methanol (9:1)]. The procedure was adapted from the literature (Brown et al., 2007; Teixeira et al., 2017b).

(8-(3,4-Dimethoxybenzamido)octyl)triphenylphosphonium bromide (11). $\eta = 84\%$. $^1\text{H NMR}$ (CDCl_3): $\delta = 1.23\text{--}1.43$ (6H, *m*, $\text{NCH}_2(\text{CH}_2)_3$), $1.57\text{--}1.71$ (6H, *m*, $\text{NCH}_2\text{CH}_2(\text{CH}_2)_3(\text{CH}_2)_2$), $3.39\text{--}3.46$ (2H, *m*, NCH_2), $3.68\text{--}3.78$ (2H, *m*, CH_2P^+), 3.87 (3H, *s*, OCH_3), 3.95 (3H, *s*, OCH_3), 6.87 (1H, *d*, $J = 8.3$ Hz, H(5)), 7.53 (1H, *s*, CO), $7.60\text{--}7.87$ (17H, *m*, H(2), H(6) and PPh_3). $^{13}\text{C NMR}$ (CDCl_3): $\delta = 22.5$ (*d*, $J_{\text{CP}} = 4.7$ Hz, $\text{CH}_2(\text{CH}_2)_2\text{P}^+$), 22.8 (*d*, $J_{\text{CP}} = 49.4$ Hz, CH_2P^+), 26.2 ($\text{N}(\text{CH}_2)_2\text{CH}_2$), 28.0 ($\text{N}(\text{CH}_2)_4\text{CH}_2$), 28.2 ($\text{N}(\text{CH}_2)_3\text{CH}_2$), 29.0 (NCH_2CH_2), 29.8 (*d*, $J_{\text{CP}} = 15.9$ Hz, $\text{CH}_2\text{CH}_2\text{P}^+$), 39.9 (NCH_2), 56.1 (OCH_3), 56.6 (OCH_3), 110.5 (C(5)), 111.1 (C(2)), 118.6 (*d*, $J_{\text{CP}} = 85.8$ Hz, $3 \times \text{C}(1')$), 120.7 (C(6)), 127.6 (C(1)), 130.6 (*d*, $J_{\text{CP}} = 12.5$ Hz, $3 \times \text{C}(3')$ and $3 \times \text{C}(5')$), 133.8 (*d*, $J_{\text{CP}} = 10.0$ Hz, $3 \times \text{C}(2')$ and $3 \times \text{C}(6')$), 135.1 (*d*, $J_{\text{CP}} = 3.0$ Hz, $3 \times \text{C}(4')$), 148.8 (C(3)), 151.4 (C(4)), 167.2 (CO). ESI/MS *m/z* (%): 555 ($[\text{M}+\text{H}-\text{Br}]^+$, 52), 554 ($[\text{M}-\text{Br}]^+$, 100).

(8-(3,4,5-Trimethoxybenzamido)octyl)triphenylphosphonium bromide (12). $\eta = 87\%$. $^1\text{H NMR}$ (CDCl_3): $\delta = 1.29\text{--}1.45$ (6H, *m*, $\text{NCH}_2(\text{CH}_2)_3$), $1.60\text{--}1.74$ (6H, *m*, $\text{NCH}_2\text{CH}_2(\text{CH}_2)_3(\text{CH}_2)_2$), $3.43\text{--}3.50$ (2H, *m*, NCH_2), $3.65\text{--}3.74$ (2H, *m*, CH_2P^+), 3.85 (3H, *s*, OCH_3), 3.95 (6H, *s*, $2 \times \text{OCH}_3$), 7.39 (2H, *s*, H(2) and H(6)), $7.66\text{--}7.83$ (15H, *m*, PPh_3), 8.12 (1H, *s*, NH). $^{13}\text{C NMR}$ (CDCl_3): $\delta = 22.4$ (*d*, $J_{\text{CP}} = 4.6$ Hz, $\text{CH}_2(\text{CH}_2)_2\text{P}^+$), 22.7 (*d*, $J_{\text{CP}} = 49.2$ Hz, CH_2P^+), 25.9 ($\text{N}(\text{CH}_2)_2\text{CH}_2$), 27.6 ($\text{N}(\text{CH}_2)_4\text{CH}_2$), 27.9 ($\text{N}(\text{CH}_2)_3\text{CH}_2$), 28.7 (NCH_2CH_2), 29.6 (*d*, $J_{\text{CP}} = 16.1$ Hz, $\text{CH}_2\text{CH}_2\text{P}^+$), 40.0 (NCH_2), 57.0 ($2 \times \text{OCH}_3$), 60.9 (OCH_3), 105.3 (C(2) and C(6)), 118.5 (*d*, $J_{\text{CP}} = 85.9$ Hz, $3 \times \text{C}(1')$), 130.5 (C(1)), 130.6 (*d*, $J_{\text{CP}} = 12.5$ Hz, $3 \times \text{C}(3')$ and $3 \times \text{C}(5')$), 133.8 (*d*, $J_{\text{CP}} = 10.0$ Hz, $3 \times \text{C}(2')$ and $3 \times \text{C}(6')$), 135.2 (*d*, $J_{\text{CP}} = 3.0$ Hz, $3 \times \text{C}(4')$), 140.4 (C(4)), 153.0 (C(3) and C(5)), 167.2 (CO). ESI/MS *m/z* (%): 585 ($[\text{M}+\text{H}-\text{Br}]^+$, 48), 584 ($[\text{M}-\text{Br}]^+$, 100).

(10-(3,4-Dimethoxybenzamido)decyl)triphenylphosphonium bromide (13). $\eta = 82\%$. $^1\text{H NMR}$ (CDCl_3): $\delta = 1.17\text{--}1.37$ (12H, *m*, $\text{NCH}_2(\text{CH}_2)_6$), $1.57\text{--}1.67$ (4H, *m*, $\text{NCH}_2\text{CH}_2(\text{CH}_2)_6\text{CH}_2$), $3.37\text{--}3.46$ (2H, *m*, NCH_2), $3.71\text{--}3.83$ (2H, *m*, CH_2P^+), 3.89 (3H, *s*, OCH_3), 3.93 (3H, *s*, OCH_3), 6.86 (1H, *d*, $J = 8.4$ Hz, H(5)), 7.00 (1H, *s*, NH), 7.48 (1H, *d*, $J = 8.4$ Hz, H(6)), 7.55 (1H, *d*, $J = 1.8$ Hz, H(2)), $7.66\text{--}7.87$ (15H, *m*, PPh_3). $^{13}\text{C NMR}$ (CDCl_3): $\delta = 22.7$ (*d*, $J_{\text{CP}} = 4.6$ Hz, $\text{CH}_2(\text{CH}_2)_2\text{P}^+$), 22.9 (*d*, $J_{\text{CP}} = 49.6$ Hz, CH_2P^+), 26.7 ($\text{N}(\text{CH}_2)_2\text{CH}_2$), 28.7 ($\text{N}(\text{CH}_2)_6\text{CH}_2$), 28.8 ($\text{N}(\text{CH}_2)_3(\text{CH}_2)_3$), 29.4 (NCH_2CH_2), 30.2 (*d*, $J_{\text{CP}} = 15.8$ Hz, $\text{CH}_2\text{CH}_2\text{P}^+$), 40.1 (NCH_2), 56.1 (OCH_3), 56.4 (OCH_3), 110.5 (C(5)), 111.0 (C(2)), 118.6 (*d*, $J_{\text{CP}} = 85.8$ Hz, $3 \times \text{C}(1')$), 120.2 (C(6)), 127.5 (C(1)), 130.6 (*d*, $J_{\text{CP}} = 12.5$ Hz, $3 \times \text{C}(3')$ and $3 \times \text{C}(5')$), 133.8 (*d*, $J_{\text{CP}} = 9.9$ Hz, $3 \times \text{C}(2')$ and $3 \times \text{C}(6')$), 135.1 (*d*, $J_{\text{CP}} = 2.9$ Hz, $3 \times \text{C}(4')$), 148.9 (C(3)), 151.5 (C(4)), 167.2 (CO). ESI/MS *m/z* (%): 583 ($[\text{M}+\text{H}-\text{Br}]^+$, 38), 582 ($[\text{M}-\text{Br}]^+$, 100).

(10-(3,4,5-Trimethoxybenzamido)decyl)triphenylphosphonium bromide (14). $\eta = 92\%$. $^1\text{H NMR}$ (CDCl_3): $\delta = 1.18\text{--}1.38$ (12H, *m*, $\text{NCH}_2(\text{CH}_2)_6$), $1.56\text{--}1.64$ (4H, *m*, $\text{NCH}_2\text{CH}_2(\text{CH}_2)_6\text{CH}_2$), $3.39\text{--}3.46$ (2H, *m*, NCH_2), $3.68\text{--}3.76$ (2H, *m*, CH_2P^+), 3.84 (3H, *s*, OCH_3), 3.90 (6H, *s*, $2 \times \text{OCH}_3$), 7.27 (2H, *s*, H(2) and H(6)), 7.60 (1H, *s*, NH), $7.65\text{--}7.85$ (15H, *m*, PPh_3). $^{13}\text{C NMR}$ (CDCl_3): $\delta = 22.6$ (*d*, $J_{\text{CP}} = 4.3$ Hz, $\text{CH}_2(\text{CH}_2)_2\text{P}^+$), 22.8 (*d*, $J_{\text{CP}} = 49.9$ Hz,

CH_2P^+), 26.5 ($\text{N}(\text{CH}_2)_2\text{CH}_2$), 28.2 ($\text{N}(\text{CH}_2)_6\text{CH}_2$), 28.5 ($\text{N}(\text{CH}_2)_3(\text{CH}_2)_3$), 29.0 (NCH_2CH_2), 29.9 (*d*, $J_{\text{CP}} = 15.8$ Hz, $\text{CH}_2\text{CH}_2\text{P}^+$), 40.1 (NCH_2), 56.7 ($2 \times \text{OCH}_3$), 60.8 (OCH_3), 105.0 (C(2) and C(6)), 118.4 (*d*, $J_{\text{CP}} = 85.8$ Hz, $3 \times \text{C}(1')$), 130.3 (C(1)), 130.5 (*d*, $J_{\text{CP}} = 12.5$ Hz, $3 \times \text{C}(3')$ and $3 \times \text{C}(5')$), 133.7 (*d*, $J_{\text{CP}} = 9.9$ Hz, $3 \times \text{C}(2')$ and $3 \times \text{C}(6')$), 135.1 (*d*, $J_{\text{CP}} = 3.0$ Hz, $3 \times \text{C}(4')$), 140.3 (C(4)), 152.9 (C(3) and C(5)), 167.1 (CO). ESI/MS *m/z* (%): 613 ($[\text{M}+\text{H}-\text{Br}]^+$, 51), 612 ($[\text{M}-\text{Br}]^+$, 100).

General procedure used to obtain mitochondriotropic antioxidants (15–18).

Triphenylphosphonium salt derivative (**11–14**) (1 mmol) was dissolved in anhydrous dichloromethane (15 mL). The reaction mixture was stirred under argon and cooled at a temperature below -70°C . To this solution, boron tribromide (5–7 mmol, 1 M solution in dichloromethane) was added and the reaction was kept at -70°C for 10 min. After reaching room temperature, the reaction was continued for 12 h. Thereafter, the reaction was finished by cautious addition of water (40 mL). After removing the water, the product was dissolved in methanol and the solvent evaporated. The residue was purified by cellulose flash chromatography using gradient elution (dichloromethane:methanol from 9:1 to 6:4). The fractions containing the desired compound were collected and the solvent was evaporated to dryness. The reaction was followed by TLC [silica gel, mobile phase with dichloromethane:methanol (9:1)]. The procedure was adapted from the literature (Milhazes et al., 2006; Teixeira et al., 2012, 2017a).

(8-(3,4-Dihydroxybenzamido)octyl)triphenylphosphonium bromide (15). $\eta = 82\%$. $^1\text{H NMR}$ ($\text{DMSO}-d_6$): $\delta = 1.13\text{--}1.35$ (6H, *m*, $\text{N}(\text{CH}_2)_2(\text{CH}_2)_3$), $1.36\text{--}1.72$ (6H, *m*, $\text{NCH}_2\text{CH}_2(\text{CH}_2)_3(\text{CH}_2)_2$), $3.09\text{--}3.20$ (2H, *m*, NCH_2), $3.49\text{--}3.63$ (2H, *m*, CH_2P^+), 6.74 (1H, *d*, $J = 8.2$ Hz, H(5)), 7.16 (1H, *dd*, $J = 2.0, 8.2$ Hz, H(6)), 7.26 (1H, *d*, $J = 2.0$ Hz, H(2)), $7.71\text{--}7.93$ (15H, *m*, PPh_3), 8.09 (1H, *s*, NH). $^{13}\text{C NMR}$ ($\text{DMSO}-d_6$): $\delta = 20.2$ (*d*, $J_{\text{CP}} = 49.9$ Hz, CH_2P^+), 21.8 (*d*, $J_{\text{CP}} = 4.4$ Hz, $\text{CH}_2(\text{CH}_2)_2\text{P}^+$), 26.3 ($\text{N}(\text{CH}_2)_2\text{CH}_2$), 28.0 ($\text{N}(\text{CH}_2)_4\text{CH}_2$), 28.4 ($\text{N}(\text{CH}_2)_3\text{CH}_2$), 29.2 (NCH_2CH_2), 29.7 (*d*, $J_{\text{CP}} = 16.5$ Hz, $\text{CH}_2\text{CH}_2\text{P}^+$), 39.0 (NCH_2), 114.8 (C(5)), 115.1 (C(2)), 118.6 (*d*, $J_{\text{CP}} = 85.6$ Hz, $3 \times \text{C}(1')$), 118.8 (C(6)), 126.0 (C(1)), 130.2 (*d*, $J_{\text{CP}} = 12.4$ Hz, $3 \times \text{C}(3')$ and $3 \times \text{C}(5')$), 133.6 (*d*, $J_{\text{CP}} = 10.1$ Hz, $3 \times \text{C}(2')$ and $3 \times \text{C}(6')$), 134.9 (*d*, $J_{\text{CP}} = 2.8$ Hz, $3 \times \text{C}(4')$), 144.7 (C(3)), 148.1 (C(4)), 166.0 (CO). ESI/MS *m/z* (%): 527 ($[\text{M}+\text{H}-\text{Br}]^+$, 55), 526 ($[\text{M}-\text{Br}]^+$, 100). ESI/HRMS calcd for $\text{C}_{33}\text{H}_{37}\text{NO}_3\text{P}^+$ (M^+): 526.2506, found 526.2633.

(8-(3,4,5-Trihydroxybenzamido)octyl)triphenylphosphonium bromide (16). $\eta = 83\%$. $^1\text{H NMR}$ ($\text{DMSO}-d_6$): $\delta = 1.13\text{--}1.32$ (6H, *m*, $\text{N}(\text{CH}_2)_2(\text{CH}_2)_3$), $1.36\text{--}1.60$ (6H, *m*, $\text{NCH}_2\text{CH}_2(\text{CH}_2)_3(\text{CH}_2)_2$), $3.06\text{--}3.20$ (2H, *m*, NCH_2), $3.39\text{--}3.66$ (5H, *m*, CH_2P^+ and $3 \times \text{OH}$), 6.80 (2H, *s*, H(2) and H(6)), $7.71\text{--}7.93$ (15H, *m*, PPh_3), 7.99 (1H, *s*, NH). $^{13}\text{C NMR}$ ($\text{DMSO}-d_6$): $\delta = 20.1$ (*d*, $J_{\text{CP}} = 49.3$ Hz, CH_2P^+), 21.7 (*d*, $J_{\text{CP}} = 4.2$ Hz, $\text{CH}_2(\text{CH}_2)_2\text{P}^+$), 26.3 ($\text{N}(\text{CH}_2)_2\text{CH}_2$), 28.0 ($\text{N}(\text{CH}_2)_4\text{CH}_2$), 28.4 ($\text{N}(\text{CH}_2)_3\text{CH}_2$), 29.1 (NCH_2CH_2), 29.7 (*d*, $J_{\text{CP}} = 16.4$ Hz, $\text{CH}_2\text{CH}_2\text{P}^+$), 38.9 (NCH_2), 106.7 (C(2) and C(6)), 118.6 (*d*, $J_{\text{CP}} = 85.6$ Hz, $3 \times \text{C}(1')$), 125.2 (C(1)), 130.2 (*d*, $J_{\text{CP}} = 12.4$ Hz, $3 \times \text{C}(3')$ and $3 \times \text{C}(5')$), 133.6 (*d*, $J_{\text{CP}} = 10.1$ Hz, $3 \times \text{C}(2')$ and

$3 \times C(6')$, 134.9 (*d*, $J_{CP} = 2.8$ Hz, $3 \times C(4')$), 136.0 (C(4)), 145.3 (C(3) and C(5)), 166.2 (CO). ESI/MS *m/z* (%): 543 ([M+H-Br]⁺, 100), 542 ([M-Br]⁺, 59). ESI/HRMS calcd for C₃₃H₃₇NO₄P⁺ (M⁺): 542.2455, found 542.2412.

(10-(3,4-Dihydroxybenzamido)decyl)triphenylphosphonium bromide (17). $\eta = 69\%$. ¹H NMR (DMSO-*d*₆): $\delta = 1.11$ – 1.30 (10H, *m*, N(CH₂)₂(CH₂)₅), 1.36 – 1.61 (6H, *m*, NCH₂CH₂(CH₂)₅(CH₂)₂), 3.10 – 3.25 (2H, *m*, NCH₂), 3.46 – 3.62 (4H, *m*, CH₂P⁺ and $2 \times$ OH), 6.73 (1H, *d*, $J = 8.2$ Hz, H(5)), 7.16 (1H, *dd*, $J = 2.1$, 8.2 Hz, H(6)), 7.25 (1H, *d*, $J = 2.1$ Hz, H(2)), 7.74 – 7.91 (15H, *m*, PPh₃), 8.07 (1H, *t*, $J = 5.6$ Hz, NH). ¹³C NMR (DMSO-*d*₆): $\delta = 20.1$ (*d*, $J_{CP} = 50.2$ Hz, CH₂P⁺), 21.7 (*d*, $J_{CP} = 4.7$ Hz, CH₂(CH₂)₂P⁺), 26.5 (N(CH₂)₂CH₂), 28.0 (N(CH₂)₆CH₂), 28.6 (N(CH₂)₃CH₂), 28.7 (N(CH₂)₅CH₂), 28.8 (N(CH₂)₄CH₂), 29.2 (NCH₂CH₂), 29.8 (*d*, $J_{CP} = 16.4$ Hz, CH₂CH₂P⁺), 39.0 (NCH₂), 114.7 (C(5)), 115.0 (C(2)), 118.6 (*d*, $J_{CP} = 85.6$ Hz, $3 \times$ C(1')), 118.8 (C(6)), 126.0 (C(1)), 130.2 (*d*, $J_{CP} = 12.4$ Hz, $3 \times$ C(3')) and $3 \times$ C(5')), 133.6 (*d*, $J_{CP} = 10.1$ Hz, $3 \times$ C(2')) and $3 \times$ C(6')), 134.9 (*d*, $J_{CP} = 3.0$ Hz, $3 \times$ C(4')), 144.7 (C(3)), 148.1 (C(4)), 165.9 (CO). ESI/MS *m/z* (%): 555 ([M+H-Br]⁺, 58), 554 ([M-Br]⁺, 100). ESI/HRMS calcd for C₃₅H₄₁NO₃P⁺ (M⁺): 554.2819, found 554.2821.

(10-(3,4,5-Trihydroxybenzamido)decyl)triphenylphosphonium bromide (18). $\eta = 89\%$. ¹H NMR (DMSO-*d*₆): $\delta = 1.02$ – 1.30 (10H, *m*, N(CH₂)₂(CH₂)₅), 1.34 – 1.59 (6H, *m*, NCH₂CH₂(CH₂)₅(CH₂)₂), 3.06 – 3.20 (2H, *m*, NCH₂), 3.46 – 3.64 (2H, *m*, CH₂P⁺), 6.80 (2H, *s*, H(2) and H(6)), 7.69 – 7.93 (15H, *m*, PPh₃), 8.00 (1H, *s*, NH). ¹³C NMR (DMSO-*d*₆): $\delta = 20.2$ (*d*, $J_{CP} = 50.1$ Hz, CH₂P⁺), 21.7 (*d*, $J_{CP} = 4.2$ Hz, CH₂(CH₂)₂P⁺), 26.4 (N(CH₂)₂CH₂), 28.0 (N(CH₂)₆CH₂), 28.6 (N(CH₂)₃CH₂), 28.7 (N(CH₂)₅CH₂), 28.8 (N(CH₂)₄CH₂), 29.2 (NCH₂CH₂), 29.7 (*d*, $J_{CP} = 16.4$ Hz, CH₂CH₂P⁺), 39.0 (NCH₂), 106.7 (C(2) and C(6)), 118.6 (*d*, $J_{CP} = 85.6$ Hz, $3 \times$ C(1')), 125.2 (C(1)), 130.2 (*d*, $J_{CP} = 12.4$ Hz, $3 \times$ C(3')) and $3 \times$ C(5')), 133.6 (*d*, $J_{CP} = 10.1$ Hz, $3 \times$ C(2')) and $3 \times$ C(6')), 134.9 (*d*, $J_{CP} = 2.8$ Hz, $3 \times$ C(4')), 136.0 (C(4)), 14537 (C(3) and C(5)), 166.2 (CO). ESI/MS *m/z* (%): 571 ([M+H-Br]⁺, 100), 570 ([M-Br]⁺, 13). ESI/HRMS calcd for C₃₅H₄₁NO₄P⁺ (M⁺): 570.2768, found 570.2885.

Evaluation of Radical Scavenging Activity

The radical scavenging activity of compounds **AntiOxBEN**₁, **AntiOxBEN**₂, and **15–18** was evaluated using the total antioxidant capacity spectrophotometric assays based on the DPPH[•] (2,2'-diphenyl-1-picrylhydrazyl) and ABTS^{•+} (2,2'-azino-bis(3-ethylbenzthiazoline-6-sulfonic acid)) radicals.

DPPH[•] radical assay

DPPH[•] radical scavenging activity was evaluated as previously described (Teixeira et al., 2017b). The IC₅₀ values were determined in triplicate from the dose-response inhibition curves and are expressed as mean \pm standard deviation (SD).

ABTS^{•+} radical cation assay

ABTS^{•+} scavenging activity was evaluated as previously described (Teixeira et al., 2017b). The IC₅₀ values were

determined in triplicate from the dose-response inhibition curves and are expressed as mean \pm standard deviation (SD).

Evaluation of Redox Properties

Voltammetric studies were performed using an Autolab PGSTAT12 potentiostat/galvanostat (Metrohm Autolab, Netherland) and a one-compartment glass electrochemical cell. Voltammetric curves were recorded at room temperature using a three-electrode system, according the conditions previously described (Teixeira et al., 2017b).

Pharmacology

Reagents and General Conditions

Acetylcholinesterase (AChE) from *Electrophorus electricus* (electric eel), butyrylcholinesterase (BChE) and acetylthiocholine iodide (ATCI), butyrylthiocholine iodide (BTCI), 5,5'-dithiobis-(2-nitrobenzoate) (DTNB), (4,5-dimethylthiazol-2-yl)-2,5-diphenyl tetrazolium (MTT) bromide and Dulbecco's modified Eagle's medium (DMEM) with 4.5 g/L glucose were obtained from Sigma-Aldrich Quimica S. A. Reagents used in cell culture, including nonessential amino acids (NEAA), heat inactivated fetal bovine serum (FBS), 0.05% trypsin/1 mM EDTA, antibiotic (10000 U/mL penicillin, 10,000 μ g/mL streptomycin) and Hank's balanced salt solution (HBSS) were purchased from Gibco Laboratories. Dimethylsulfoxide (DMSO-*d*₆), absolute ethanol and acetic acid were obtained from Merck. All reagents were of analytical grade or of the highest grade available.

Evaluation of Acetyl and Butyrylcholinesterase Inhibitory Activity

The AChE and BChE inhibitory activities of the compounds under study were evaluated following Ellman's method (Ellman et al., 1961; Di Giovanni et al., 2008). The solutions of enzyme (AChE, 0.5 U/mL; BChE, 0.25 U/mL) and DTNB (2.14 mM) were prepared in sodium phosphate buffer. ATCI (8.04 mM) or BTCI (5.12 mM) solutions were prepared in deionised water (conductivity $< 0.1 \mu$ S·cm⁻¹).

Briefly, 100 μ L of sodium phosphate buffer, 40 μ L of DTNB, 20 μ L of the test compounds/standard inhibitors and 20 μ L of AChE or BChE were incubated for 5 min at 30°C in a 96-well microplate (BRANDplates, pureGradeTM, BRAND GMBH, Wertheim, Germany). After that, 20 μ L of ATCI or BTCI was added, respectively. The absorbance values were registered every minute for 5 more minutes at 30°C (at 412 nm). A control using 20 μ L of sodium phosphate buffer instead of compound solution was also performed. The IC₅₀ values were determined in triplicate from the dose-response inhibition curves and are expressed as mean \pm standard deviation (SD).

Evaluation of enzyme (AChE and BChE) kinetics.

To determine the steady-state kinetic parameters (K_m , Michaelis constant and V_{max} , maximum reaction rate) of AChE and BChE, their enzymatic activities were evaluated (under the experimental conditions described above) in the presence of different ATCI or BTCI concentrations. Under our experimental conditions, AChE displayed a K_m of $117.3 \pm 29.7 \mu$ M and a V_{max} of 0.27 ± 0.03

$\Delta A/\text{min}$ whereas BChE showed a K_m of $244.4 \pm 15.0 \mu\text{M}$ and a V_{max} of $0.2772 \pm 0.0007 \Delta A/\text{min}$ (determined in triplicate).

Evaluation of AChE- and BChE-inhibitor kinetics

To evaluate the mechanism of AChE and BChE inhibition of the most promising compounds substrate-dependent kinetic experiments were performed. The catalytic rates of AChE were measured at five different concentrations of ATCI substrate ($50\text{--}800 \mu\text{M}$) and BChE at four different concentrations of BTCI substrate ($62.5\text{--}500 \mu\text{M}$) in the absence or presence of the selected inhibitors (compounds **18** and **AntiOxBEN₁**) and standard inhibitor (donepezil, at concentrations between 12.5 nM and $40.0 \mu\text{M}$). The results are presented as double reciprocal Lineweaver-Burk plots ($1/V$ vs. $1/[S]$). The kinetic data, namely K_m and V_{max} , were acquired employing Michaelis-Menten equation. The K_i values were estimated using Dixon plots, by replotting the slope of each Lineweaver-Burk plot vs. the inhibitor concentration. In the Dixon plots, the K_i value was obtained from the x-axis intercept ($-K_i$). The enzymatic reactions and measurements were performed using the same AChE and BChE assay conditions as described above (determined in triplicate). Linear regression analysis was performed using GraphPad Prism 5.0 (GraphPad Software, Inc.).

Evaluation of Cytotoxicity/Antioxidant Outline in Cell-Based Assays

Cell Culture

SH-SY5Y (ATCC, Manassas, VA, USA), a neuroblastoma cell line, was routinely cultured in 75-cm^2 flasks (Corning Costar, Corning, NY, USA) using DMEM with 4.5 g/L glucose, supplemented with 10% heat-inactivated FBS (v/v), 1% NEAA (v/v), 100 U/mL penicillin, and $100 \mu\text{g/mL}$ streptomycin. The cells used for all the experiments were taken between the 37th and 45th passages, to avoid phenotypic changes. For all experiments, undifferentiated SH-SY5Y cells were seeded onto 96-well plates ($8,000$ cells/well) in cell culture medium supplemented with 0.1% of retinoic acid for 3 days at 37°C for differentiated cells. Three days after seeding, the medium of cells was changed, adding cell culture medium with 0.1% of TPA for more 3 days before treatment.

Human hepatocellular carcinoma cells (HepG2, ECACC, UK) were also used in this study. Cells were cultured in low-glucose medium (5 mM) composed by Dulbecco's modified Eagle's medium (DMEM, D5030) supplemented with sodium pyruvate (0.11 g/L), sodium bicarbonate (3.7 g/L), HEPES (1.19 g/L), 6 mM glutamine and 10% fetal bovine serum (FBS) and 1% of antibiotic penicillin-streptomycin $100 \times$ solution. HepG2 (2.5×10^4 cells/well) cells were seeded in a 96-well plate and proliferate for 24 h before treatment.

All cells were maintained and cultured at 37°C in a humidified atmosphere of 95% air/5% CO_2 and passaged weekly by trypsinization (0.05% trypsin/1 mM EDTA) when reaching 70–80% confluence.

Evaluation of Cytotoxicity

The cytotoxicity profile of the compounds under study was evaluated in differentiated SH-SY5Y cells ($8,000$ cells/well),

according the differentiation protocol previously described, and in HepG2 cells (2.5×10^4 cells/well), seeded into 96-well plates. Then, the cells were exposed to increased concentrations of the test compounds (1, 10 and $50 \mu\text{M}$) in cell culture medium for 24 h in SH-SY5Y cells or 48 h in HepG2 cells and the cytotoxicity was evaluated through measuring changes in cellular metabolic activity using the MTT or resazurin reduction assays, respectively (Silva et al., 2016). In both assays, the reduction of MTT tetrazolium salt or resazurin to MTT formazan or resorufin, respectively, by cellular dehydrogenases present in viable cells, gives insights on cell metabolic activity.

For the MTT assay, the cell culture medium was removed after the incubation time, followed by the addition of fresh cell culture medium containing 0.5 mg/mL MTT and incubation for 30 min. After this incubation period, the cell culture medium was removed, and the formed formazan crystals dissolved in DMSO. The absorbance was measured at 550 nm in a multi-well plate reader (BioTek Instruments, Vermont, USA). The percentage of MTT reduction relative to that of the control cells was used as the cytotoxicity measure [MTT reduction (% of control)] as means \pm SEM of four independent experiments.

Regarding the resazurin reduction assay, after the incubation time, the medium was replaced by fresh medium containing resazurin ($10 \mu\text{g/mL}$) prepared in sterile PBS (1X) and left to react for 1 h. The fluorescent signal was monitored using a 540 nm excitation wavelength and 590 nm emission wavelength in a Cytation 3 reader (BioTek Instruments Inc., USA). The percentage of resazurin reduction relative to that of the control cells was used as the cytotoxicity measure [resazurin reduction (% of control)] as means \pm SEM of four independent experiments.

Control experiments were performed for both viability endpoints by adding vehicle (medium with 0.1% DMSO) instead of the compound solution.

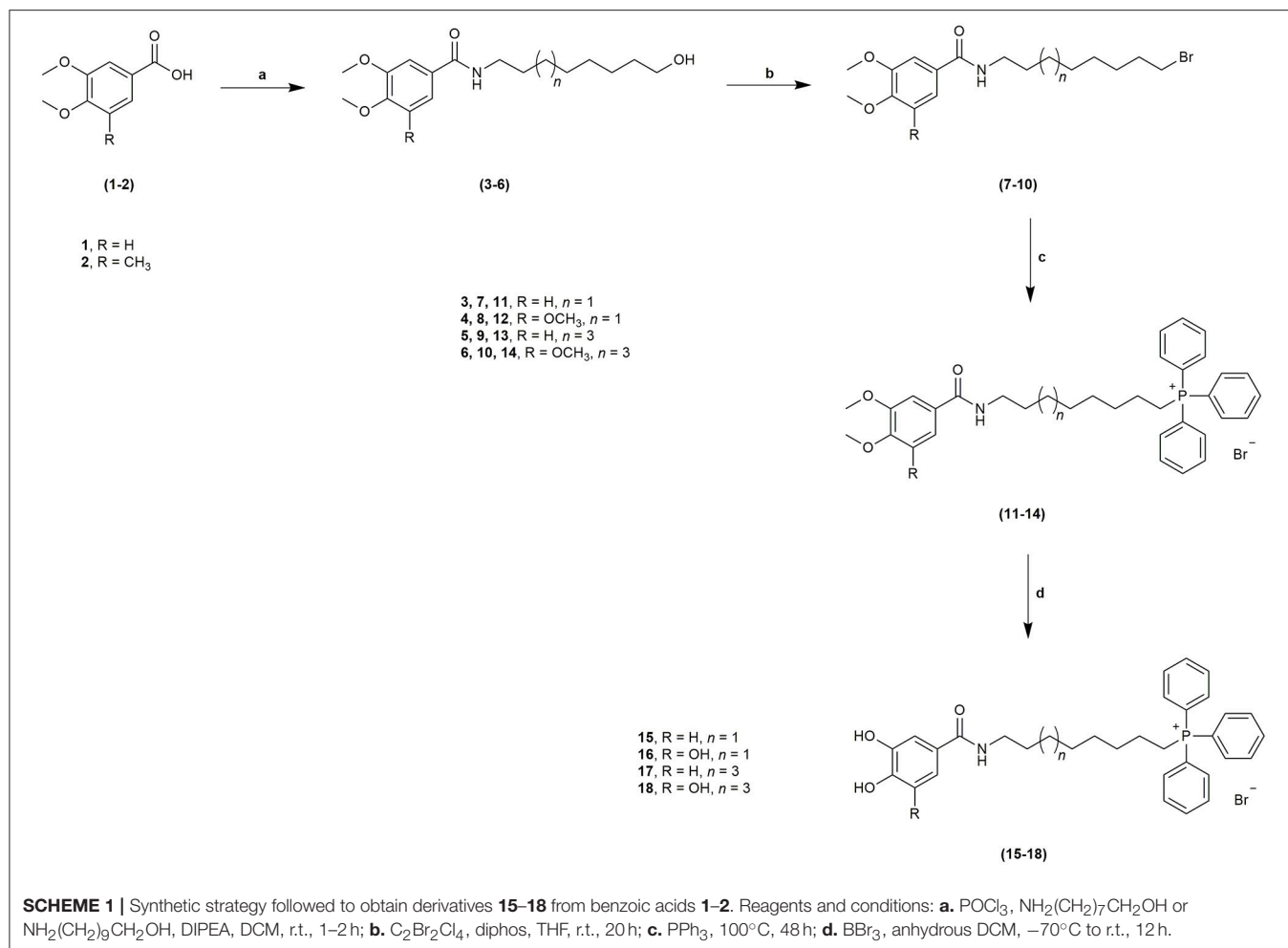
Evaluation of neuroprotective activity

The antioxidant efficiency of the new HBAC derivatives was evaluated in the presence of $\text{A}\beta_{1-42}$ peptide. The synthetic peptide $\text{A}\beta_{1-42}$, corresponding to neurotoxic amino acid residues of the human amyloid-beta protein ($\text{A}\beta$), was dissolved in sterile water in order to facilitate peptide solubilization at a concentration of 1 g/L ($221.5 \mu\text{M}$). $\text{A}\beta_{1-42}$ aliquots were then stored at -20°C until use (enriched oligomeric $\text{A}\beta_{1-42}$ preparation).

Undifferentiated SH-SY5Y cells were seeded onto 96-well plates (8000 cells/well) and differentiated as previously described. The cells were incubated with **AntiOxBEN₁**, **AntiOxBEN₂** and **15–18** ($10 \mu\text{M}$) for 24 h. Then, oligomeric $\text{A}\beta_{1-42}$ ($25 \mu\text{mol/L}$) was added to the culture medium of the SH-SY5Y cells for more 48 h. After incubation time, cellular metabolic activity was determined using the resazurin reduction assay as previously described.

Data Analysis

For the radical scavenging and enzymatic inhibition studies, the compounds were initially screened at $50 \mu\text{M}$. For the most potent compounds, dose-response curves were plotted and IC_{50} values were estimated by non-linear analysis. For the cytotoxicity assays,



MTT and resazurin reduction were calculated for each treatment as the % of control untreated cells and plotted in column graphs.

Data were analyzed in GraphPad Prism 5.0 software (GraphPad Software, Inc.), with all results being expressed as means \pm SEM for the number of experiments indicated. In data analysis, student's *t*-test was used for comparison of two means, and one-way ANOVA with Dunnett multiple comparison post-test was used to compare more than two groups with one independent variable. Significance was accepted with **P* < 0.05, ***P* < 0.01, ****P* < 0.0005, *****P* < 0.0001.

Molecular Docking Studies

Docking simulations were performed with the Schrödinger 2017 package (Schrödinger suite 2017-2, 2017). The crystal structure of the human BChE was downloaded from the PDB (code: 4B0O) (Wandhammer et al., 2013) and pre-processed with the Protein Preparation Workflow (Schrödinger suite 2017-2, 2017). This procedure included steps such as addition of cap termini, optimization of hydrogens, protonation states of residues and H-bond network optimization. Only one water molecule stabilized through two hydrogen bonds with the protein (residues Asp70 and Ser79) was retained in the pocket for the simulations.

Before docking, a receptor grid was generated using the co-crystallized ligand as a center (box length = 20 Å, *van der Waals* scaling factor = 1.0, partial charge cut-off = 0.25). Ligands were docked to the protein with Glide SP (Standard Precision) (Schrödinger suite 2017-2, 2017). The best pose according to the parameter “E_{model} energy” was retained and considered representative of the calculation. The docking protocol was validated measuring the RMSD (root mean square deviation) between 5 co-crystallized ligands downloaded from the PDB and their calculated poses extracted from docking (RMSD values: 4B0O = 1.65, 4AXB = 4.26, 4BDS = 0.37, 1P0M = 3.37, 1P0P = 2.25).

RESULTS AND DISCUSSION

Chemistry

The novel HBAC derivatives were obtained following a four-step synthetic strategy depicted in **Scheme 1**, using 3,4-dimethoxybenzoic acid (**1**) and 3,4,5-trimethoxybenzoic acid (**2**) as starting compounds. The first synthetic step (**a**) was an amidation reaction of the acids **1** and **2**: phosphorus oxychloride was used as coupling agent for the introduction

TABLE 1 | Total antioxidant capacity and ChEs inhibitory activity (IC₅₀) data of compounds **AntiOxBEN₁**, **AntiOxBEN₂**, **15–18** and donepezil.

Compound	Structure	IC ₅₀ (μM ± SD)			IC ₅₀ (nM ± SD)	SI	E _p (mV)
		DPPH [•]	ABTS ^{•+}	AChE	BChE		
AntiOxBEN₁		31.0 ± 0.8*	20.7 ± 0.8*	>50	85 ± 5	> 588	219*
AntiOxBEN₂		14.0 ± 0.3*	6.5 ± 0.5*	40.5 ± 7.0	474 ± 17	86	115*
15		31.2 ± 0.9	23.5 ± 1.3	11.2 ± 0.8	106 ± 5	106	216
16		16.8 ± 1.6	6.8 ± 0.6	15.7 ± 0.9	255 ± 9	62	121
17		31.0 ± 0.6	19.4 ± 1.0	7.7 ± 0.4	195 ± 20	41	210
18		10.2 ± 1.1	7.4 ± 0.5	7.2 ± 0.5	553 ± 22	13	114
Donepezil		n.d.	n.d.	0.025 ± 0.001	2200 ± 200	0.011	n.d.

n.d.: not determined.

*Data from Teixeira et al. (2017a).

SI: BChE selectivity index = IC₅₀(AChE)/IC₅₀(BChE).

of the 8-aminoctan-1-ol and 10-aminodecan-1-ol spacers leading to derivatives **3–6**. Subsequently, these derivatives were treated with 1,2-dibromotetrachloroethane and 1,2-bis(diphenylphosphine)ethane (diphos) (step **b**), leading to halogenated derivatives **7–10**. The triphenylphosphonium salts **11–14** were then obtained by a reaction with triphenylphosphine in step **c**, followed by a final *O*-demethylation process (step **d**) to afford derivatives **15–18**. Using this synthetic strategy, four derivatives were obtained, bearing different spacer lengths and number of phenolic functions at the aromatic ring.

The structural identity was confirmed by nuclear magnetic resonance (NMR) spectroscopy (¹H NMR, ¹³C NMR and DEPT135) and electron impact (EI/MS) or electrospray ionization mass spectra (ESI/MS).

Evaluation of Radical Scavenging Activity

Total antioxidant capacity assays (DPPH[•] and ABTS^{•+}) were used to evaluate the antioxidant capacity of compounds **15–18**. In these assays, the ability of an antioxidant to transfer a hydrogen atom or an electron to a stable free radical is related with a radical absorbance decrease and, consequently, compounds with

TABLE 2 | Drug-like properties of compounds AntiOxBEN₁, AntiOxBEN₂, 15–18 and donepezil.

Compound	MW ^a	clog P ^a	tPSA (Å ²) ^a	HBA ^a	HBD ^a	nrotb ^a	log BB ^a
AntiOxBEN ₁	498.6	6.49	69.56	4	3	12	−0.588
AntiOxBEN ₂	514.6	5.81	89.79	5	4	12	−0.665
15	526.6	6.93	69.56	4	3	14	−0.594
16	542.6	6.31	89.79	5	4	14	−0.675
17	554.7	7.32	69.56	4	3	16	−0.600
18	570.7	6.74	89.79	5	4	16	−0.685
Donepezil	379.5	3.54	38.77	4	0	6	0.790
CNS ⁺ drugs (Pajouhesh and Lenz, 2005; Hitchcock and Pennington, 2006; Fong, 2015; Rankovic, 2015; Nikolic et al., 2016)	<450	<5	<60–70	<7	<3	<8	≥−1

^aProperties calculated using StarDrop software. MW, molecular weight; clogP: logarithm of the octanol-water partition coefficient; tPSA, topological polar surface area; HBA, number of hydrogen acceptors; HBD, number of hydrogen donors; nrotb, number of rotatable bonds; log BB, logarithm of the ratio of the concentration of a drug in the brain and in the blood.

a higher antioxidant activity display a lower IC₅₀ value. The data related with AntiOxBEN₁ and AntiOxBEN₂ (Figure 1) was previously published, and included for comparative analysis (Teixeira et al., 2017b).

Results showed that pyrogallol derivatives AntiOxBEN₂, 16, 18 displayed a superior antioxidant activity over the corresponding catechols AntiOxBEN₁, 15, 17 (Table 1). Although the length of the carbon alkyl chain did not alter the antioxidant capacity of the synthesized HBAC derivatives, the presence of the TPP⁺ moiety decreased their antioxidant capacity, a fact that may be related with stereochemical hindrances.

Evaluation of Redox Properties

During the last decade, electrochemical methods have attracted a great deal of attention given their enormous potential for the assessment of antioxidant capacity. Since antioxidants can act as reducing agents, they are electrochemically active and can be measured using electrochemical techniques (Teixeira et al., 2017a,b; Apak et al., 2018). Moreover, these methods provide a fast, simple and a low-cost alternative to measure antioxidant compounds and monitor their antioxidant capacity in biological and food samples (Teixeira et al., 2017a,b; Apak et al., 2018).

The oxidative profile of compounds 15–18 was evaluated at physiological pH 7.4, by differential pulse and cyclic voltammetry, using a glassy carbon working electrode. The DPV voltammograms obtained for catechol derivatives (15 and 17) showed the occurrence of only one anodic peak at an oxidation potential (E_p) between + 210 and + 216 mV (Table 1) at physiological pH. Cyclic voltammograms were also recorded for these derivatives and the data obtained was characteristic of an electrochemical reversible reaction showing only one anodic peak and one cathodic peak on the reverse scan. DPV of the compounds containing a pyrogallol moiety (16 and 18) were also obtained and showed the presence of two overlapped anodic waves occurring at an E_p ranging from + 114 to + 121 mV, at physiological pH (Table 1). The cyclic voltammograms also showed the presence of two overlapped peaks with no reduction peak on the cathodic sweep, indicating that the oxidative process may correspond to an irreversible reaction.

The results were in accordance with the data previously obtained for AntiOxBEN₁, AntiOxBEN₂ and their parent HBAC (PA and GA) (Teixeira et al., 2017b) reinforcing our believe that the redox potential of these mitochondriotropic antioxidants is mainly associated with the number of hydroxyl substituents on the aromatic pattern. Furthermore, the data showed that the oxidation potentials observed are closely related to the antioxidant activity evaluated by total antioxidant assays. In fact, pyrogallol derivatives that presented lower oxidation potentials, exhibited higher antioxidant activities when compared with compounds bearing a catechol group (Table 1). On the other hand, the results showed that the increase of the length of alkyl spacer does not significantly influence the redox properties of the compounds, under the experimental conditions used.

Evaluation of AChE/BChE Inhibitory Activities

The inhibitory activity of the compounds AntiOxBEN₁, AntiOxBEN₂, and 15–18 on AChE and BChE was evaluated by the Ellman's method (Ellman et al., 1961; Di Giovanni et al., 2008). ATCI and BTCI were used as substrates for AChE or BChE, respectively, generating thiocholine and acetate or butyrate. In this assay, the released thiocholine reacts with the ion DTNB to produce the anion 5-thio-2-nitrobenzoate (TNB^{2−}), which was determined by UV/Vis spectroscopy (Ellman et al., 1961; Di Giovanni et al., 2008), enabling the determination of the inhibitory potency (IC₅₀ values) after incubation with the test compounds (Table 1). Donepezil (Table 1) a selective and reversible AChE inhibitor drug approved by FDA for AD treatment (Colović et al., 2013) was used as standard.

With the exception of AntiOxBEN₁, which did not have any effect on AChE at 50 μM, all derivatives effectively inhibited both AChE and BChE under the experimental conditions. Concerning AChE, derivatives presenting the longer spacers showed improved binding to the enzyme's active site. In fact, compounds 17 and 18, with a ten-carbon chain, showed greater potency (IC₅₀ = 7.7 and 7.2 μM, respectively) than AntiOxBEN₁, AntiOxBEN₂ (IC₅₀ = > 50 and 40.5 μM, respectively) and derivatives 15–16 (IC₅₀ = 11.2 and 15.7 μM, respectively) (Table 1). The compounds with

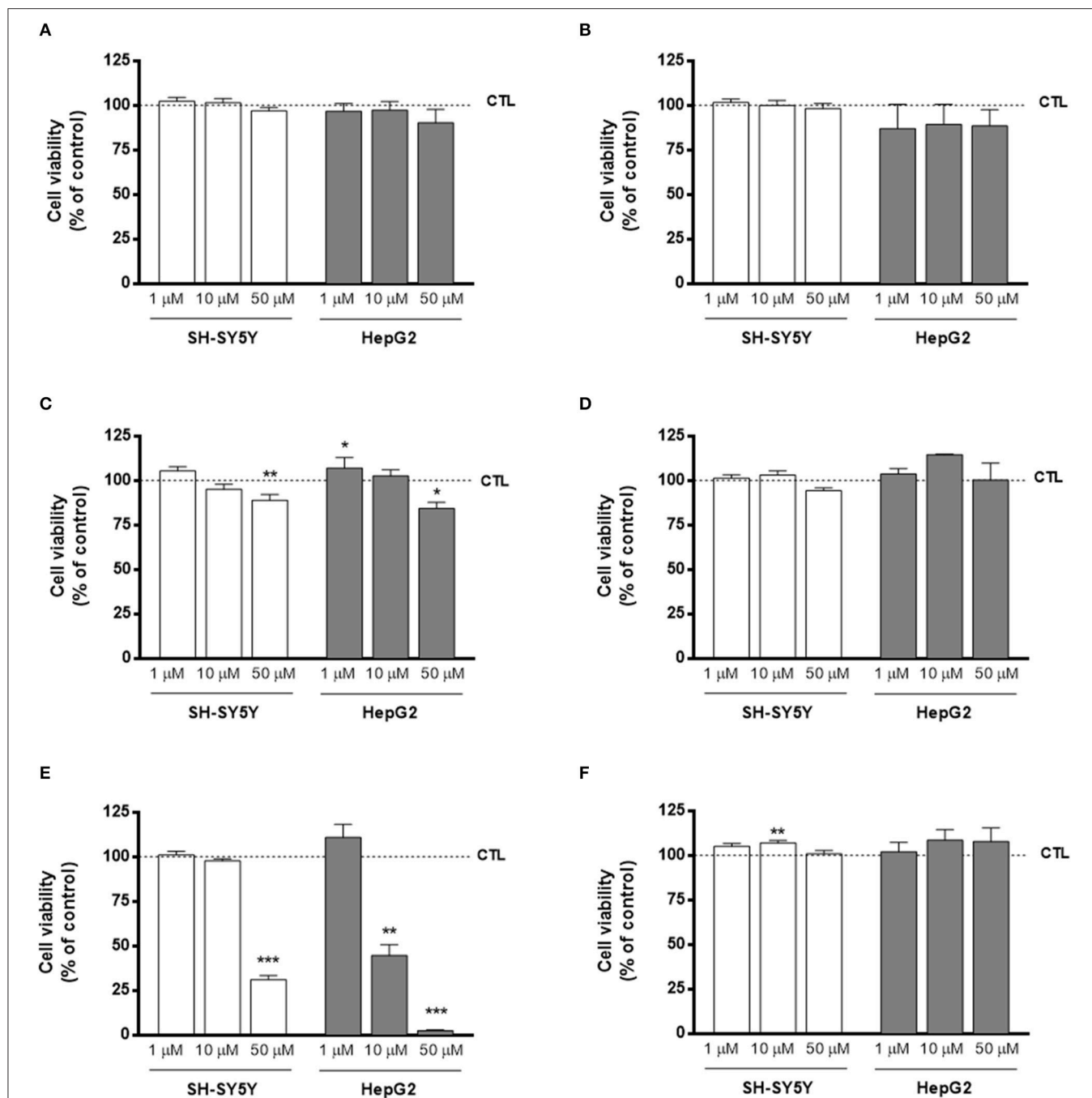


FIGURE 2 | Cytotoxicity profile of compounds (A) AntiOxBEN₁, (B) AntiOxBEN₂, (C) 15, (D) 16, (E) 17, and (F) 18 measured by changes in cellular metabolic activity on human neuroblastoma SH-SY5Y and human hepatocarcinoma HepG2 cells after 24 or 48 h treatment time, respectively, at three different concentrations (1, 10, and 50 μM). Cellular viability was evaluated using two methods: MTT in differentiated SH-SY5Y and resazurin reduction assays in HepG2 cells. Untreated cells were used as control. Data are means ± SEM of three independent experiments and the results are expressed as percentage of control (control = 100%), which represents the cell density without any treatment in the respective time point. Significance was accepted with **P* < 0.05, ***P* < 0.01, ****P* < 0.0005 vs. control.

shorter alkyl spacers (AntiOxBEN₁, 15 and 16) showed higher inhibitory potency toward BChE (IC_{50} = 85, 106 and 255 nM, respectively).

Catechol derivatives AntiOxBEN₁, 15 and 17 (IC_{50} = 85–190 nM) showed better performance than pyrogallols AntiOxBEN₂, 16 and 18 (IC_{50} = 255–550 nM).

As expected donepezil showed a higher potency for AChE than BChE (IC_{50} = 25 ± 1 nM and 2.2 ± 0.2 μM, respectively).

The BChE selectivity index (SI) calculated from the ratio of the IC_{50} values of AChE and BChE showed that the most selective compounds were AntiOxBEN₁ and 15 (over 588- and 106-fold more active toward BChE than AChE, respectively). Thus,

the modifications performed in PA significantly increased their inhibitory effect in BChE.

Evaluation of Drug-Like Properties

The drug-like properties were determined for compounds **AntiOxBEN₁**, **AntiOxBEN₂**, **15–18**, donepezil and precursors PA and GA. The calculated physicochemical parameters included: molecular weight (MW), partition coefficient (log P), topological polar surface area (tPSA in Å²), number of hydrogen acceptors (HBA), number of hydrogen donors (HBD), number of rotatable bonds (*n*rotb) and blood (plasma)-brain partitioning (logBB) (Table 2). Along theoretical calculations of logP, it was observed that the programs used do not include ionic compounds (as mitochondriotropic salts). Therefore, all the calculations were done with the neutral molecule, resulting in higher partition coefficients than expected. Due to the high volume of the aliphatic TPP⁺ moiety, the MW and logP values overcome the upper limit established by the “Rule of 5” (MW ≤ 500 g/mol and logP ≤ 5) (Lipinski et al., 2001). However, this problem can be counterbalanced by its therapeutic profile, i.e., the ability of TPP⁺ moiety to rapidly cross phospholipid bilayers and, consequently, accumulate in mitochondria (Murphy and Smith, 2007).

The values of HBD and HBA obtained were in accordance with the general drug-likeness requirements of the Lipinski’s “Rule of 5” (with HBD < 5 and HBA < 10) (Lipinski et al., 2001).

Another key measurement is the prediction of blood-brain barrier (BBB) permeability, determined by the logBB, which is the ratio of the steady-state concentrations of the drug in the brain and in the blood. Compounds with logBB < −1 are poorly distributed to the brain and are unlikely to function as effective central nervous system (CNS) drugs (Clark, 1999). Compounds **AntiOxBEN₁**, **AntiOxBEN₂**, and **15–18** displayed logBB ≥ −1, pointing toward potential BBB permeability.

As expected, the values obtained for donepezil were all in accordance with the general drug-likeness requirements of the Lipinski’s “Rule of 5.”

Evaluation of Cytotoxicity Profile

The cytotoxicity profile of compounds **AntiOxBEN₁**, **AntiOxBEN₂**, and **15–18** was evaluated by the determination of the cellular metabolic activity in differentiated human neuroblastoma cells (SH-SY5Y) and human hepatocarcinoma cells (HepG2), after a 24 or 48 h incubation period, respectively, at three different concentrations (1, 10, and 50 μM) (Figure 2). Both cell lines are often used in the preclinical safety assessment of drug candidates, being the SH-SY5Y cells of particular interest concerning the drug candidates for CNS (Lin and Will, 2012). Metabolically active cells reduce MTT and resazurin to formazan and resorufin, respectively, which can be spectrophotometrically quantified, providing an indirect measure of cell viability (Lobner, 2000). Although the **AntiOxBEN₁**, **AntiOxBEN₂** cytotoxicity on HepG2 has been previously described (Teixeira et al., 2017b), they were re-evaluated for comparative analysis.

In general, the cytotoxicity profile of all compounds followed the same trend independently of the cell line used for safety assessment. Moreover, the results clearly showed that compounds **AntiOxBEN₂**, **16** and **18**, containing the pyrogallol

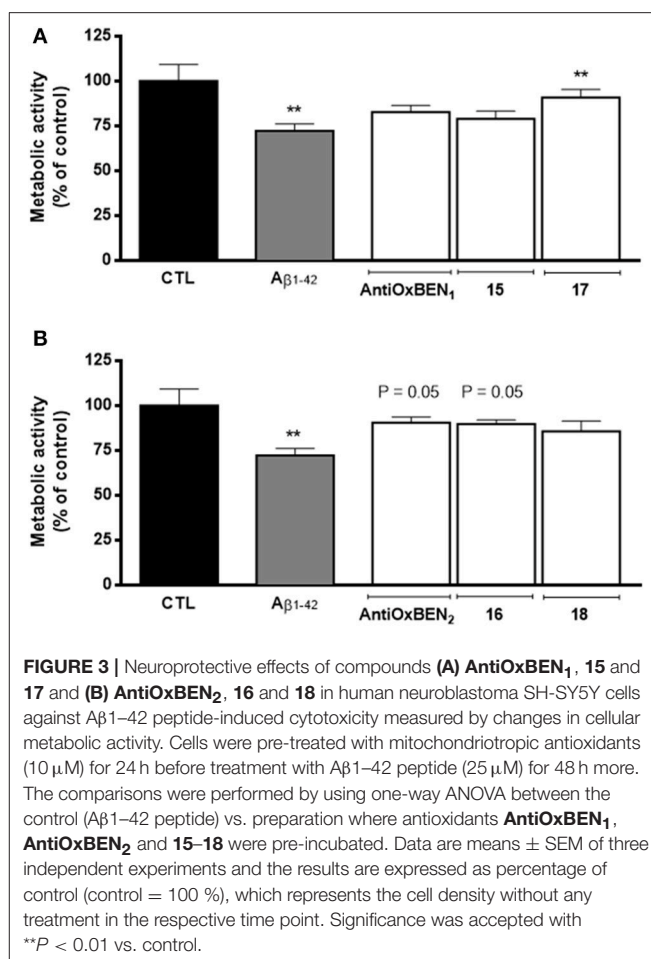


FIGURE 3 | Neuroprotective effects of compounds (A) **AntiOxBEN₁**, **15** and **17** and (B) **AntiOxBEN₂**, **16** and **18** in human neuroblastoma SH-SY5Y cells against Aβ1-42 peptide-induced cytotoxicity measured by changes in cellular metabolic activity. Cells were pre-treated with mitochondriotropic antioxidants (10 μM) for 24 h before treatment with Aβ1-42 peptide (25 μM) for 48 h more. The comparisons were performed by using one-way ANOVA between the control (Aβ1-42 peptide) vs. preparation where antioxidants **AntiOxBEN₁**, **AntiOxBEN₂** and **15–18** were pre-incubated. Data are means ± SEM of three independent experiments and the results are expressed as percentage of control (control = 100 %), which represents the cell density without any treatment in the respective time point. Significance was accepted with ***P* < 0.01 vs. control.

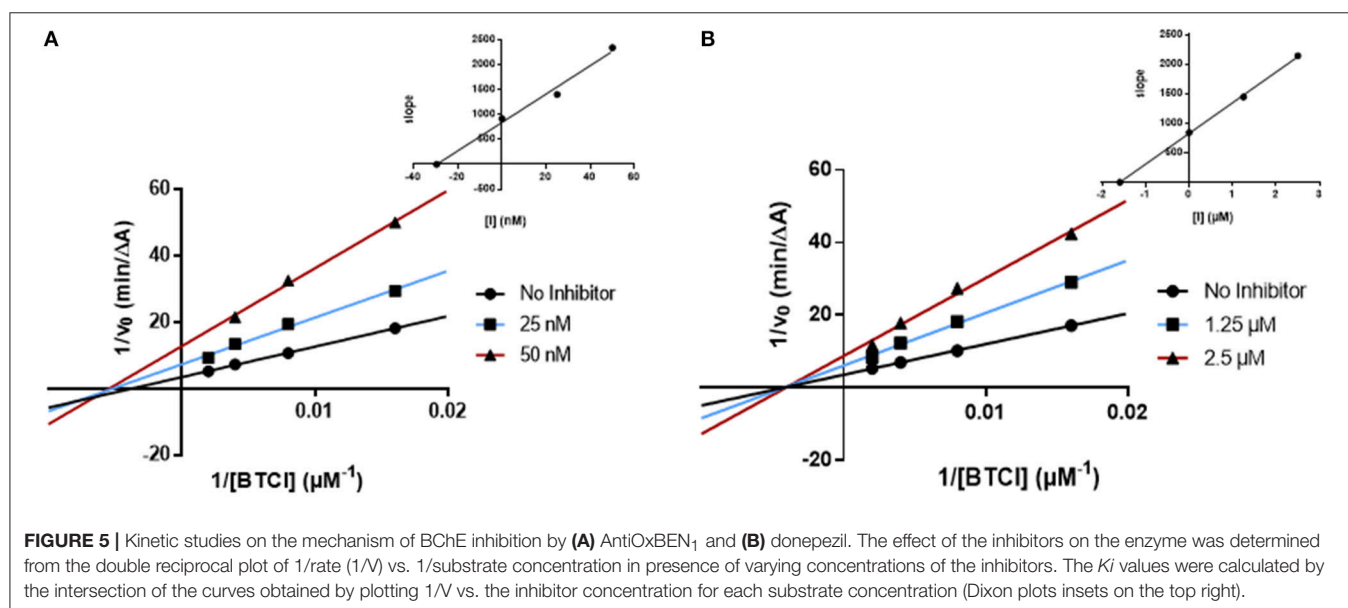
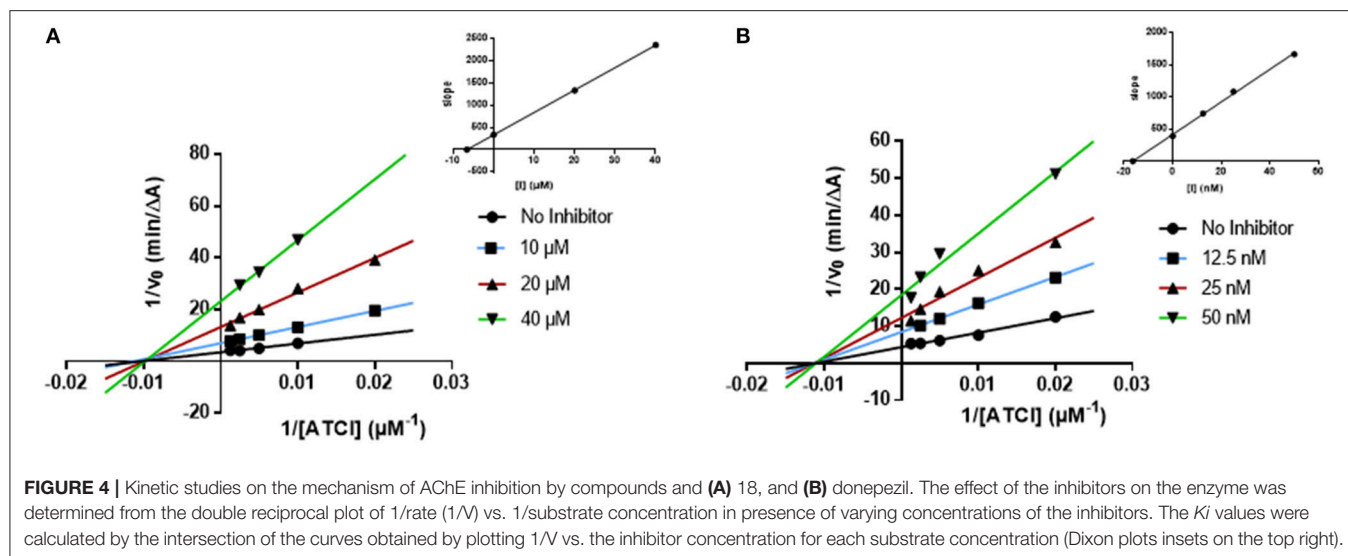
moiety, did not alter cellular metabolic activity for all tested concentrations, presenting a larger safety margin toward SH-SY5Y and HepG2 cells. Interestingly, compound **18** slightly increased SH-SY5Y (1 and 10 μM) and HepG2 (10 and 50 μM) metabolic activity.

On the other hand, compounds with the catechol moiety (**AntiOxBEN₁**, **15** and **17**) presented dose-dependent toxicity in both SH-SY5Y and HepG2 cells. Compounds **15** and **17** were the most cytotoxic compounds, showing that longer spacers increased the toxicity effects of catechol-derived compounds.

From the cytotoxic profile on both SH-SY5Y and HepG2 cells, it can be concluded that compounds containing the catechol moiety, with exception of **AntiOxBEN₁**, exhibited a higher toxicity than compounds with the pyrogallol moiety.

Evaluation of Neuroprotective Properties

Aβ aggregation, the pathological hallmark of AD, is the most targeted biomarker in drug discovery and development for AD. As ChEs colocalize with the amyloid and may contribute to the generation of amyloid proteins, it was found relevant to check the neuroprotective properties of compounds under study. The experiments were performed in SH-SY5Y cells using Aβ1-42, a synthetic toxic fragment of the amyloid protein (Resende et al.,



2008), as oxidative insult. Consequently, SH-SY5Y cells were treated with A β 1–42 peptide (25 μ M) for 48 h and then the cell metabolic activity was measured by colorimetric resazurin assay, which significantly decrease the cell viability of about 28% when compared to control.

In general, pre-treatment of SH-SY5Y cells with compounds AntiOxBEN₁, AntiOxBEN₂ and 15–18 (10 μ M, Figure 3) for 24 h reduced A β 1–42 peptide-induced cytotoxicity, being those effects more evident for compounds 17 (presenting a catechol moiety and a longer spacer) and AntiOxBEN₂ and 16 (with a pyrogallol moiety and shorter alkyl spacers) (Figure 3). Several mechanisms, such as inhibition of mitochondrial Ca²⁺ overload and of caspase cascade, may underlie HBAC derivatives-induced neuroprotection against A β neurotoxicity, which will be the subject of a follow-up study.

Evaluation of Enzyme-Inhibition Mechanism of AntiOxBEN₁ and 18

In order to understand the AChE and BChE inhibitory mechanism of the most promising ChE inhibitors, kinetic experiments were performed. For this purpose, the enzymatic inhibition kinetics was measured, using different substrate concentrations in absence or presence of the selected compounds at different concentrations, including the standard inhibitor donepezil (Figures 4, 5). Graphical analysis of the reciprocal Lineweaver–Burk plots was used to determine Michaelis–Menten reaction kinetic parameters (K_m and V_{max}).

AChE Kinetics

Concerning compound 18 (Figure 4A), results showed that V_{max} decreased while K_m remained unchanged. The same kinetic behavior was observed for donepezil (Figure 4B) (Sugimoto

TABLE 3 | E_{model} and SP scoring values for co-crystallized ligands and our set of derivatives.

Compound	E_{model}	SP score
4B0O*	-64.70	-7.81
4AXB*	-36.09	-6.97
4BDS*	-62.52	-8.18
1POM*	-34.03	-5.07
1POP*	-44.67	-5.01
AntiOxBEN ₁	-104.97	-8.58
AntiOxBEN ₂	-120.22	-9.85
15	-109.56	-9.58
16	-114.26	-9.57
17	-111.74	-9.46
18	-106.26	-8.51

*Co-crystallized ligands. Units, kcal/mol.

et al., 2002; Pohanka, 2014). The Lineweaver-Burk plots obtained for compound **18** and donepezil displayed a series of converging lines on the same point of the x-axis ($1/[S]$), profiling a non-competitive inhibition mechanism (Figure 4).

From the Dixon plots, obtained from the replots of the slopes of the Lineweaver-Burk plots vs. inhibitor concentrations (Figure 4, upper right corners), the AChE inhibition binding affinities, determined as inhibition constants (K_i), were calculated. Compound **18** (Figure 4A) displayed a K_i value of $6.6 \mu\text{M}$, which correlated well with its experimental IC_{50} ($7.2 \mu\text{M}$). The similar IC_{50} and K_i values confirmed its non-competitive inhibition profile. The kinetic inhibition profile is similar to donepezil ($K_i = 16.4 \text{ nM}$ and $\text{IC}_{50} = 24.6 \text{ nM}$, Figure 4B).

BChE Kinetics

The kinetics determined for AntiOxBEN₁ (the most selective compound) showed that the V_{max} decreased while K_m remained unchanged (Figure 5A). The same profile was obtained for donepezil (Figure 5B). The Lineweaver-Burk plots obtained for AntiOxBEN₁ and donepezil (Figures 5A,B) displayed a series of converging lines on the same point of the x-axis ($1/[S]$), profiling a non-competitive inhibition mechanism.

From the Dixon plots, obtained from the replots of the slopes of the Lineweaver-Burk plots vs. inhibitor concentrations (upper right corner), the BChE inhibition binding affinities, determined as inhibition constants (K_i), were calculated. AntiOxBEN₁ (Figure 5A) displayed K_i value of 29.5 nM and $\text{IC}_{50} = 85 \text{ nM}$. This compound displayed IC_{50} and K_i values different but in the same range, with an acceptable correlation between its respective values. Donepezil showed a similar kinetic behavior ($K_i = 1.6 \mu\text{M}$ and $\text{IC}_{50} = 2.2 \mu\text{M}$, Figure 5B).

Molecular Docking Studies

Molecular docking simulations of the best BChE inhibitors of the series were performed to study the main ligand-protein interactions. In the modeling, the crystallized human protein structure 4B0O (PDB code) was used. (Wandhammer et al., 2013). The ligands were docked with Glide SP mode (Schrödinger suite 2017-2, 2017) and the best pose according to the energetic

parameter E_{model} was retained for graphical purposes (see Table 3 with SP and E_{model} values). The geometrical quality of the docking protocol was evaluated measuring the RMSD between co-crystallized ligands and theoretical poses extracted from docking (see Methods).

The RMSD values were lower than 2.5 \AA for 3 out of 5 co-crystallized ligands showing the ability of the docking to reproduce some co-crystallized structures. For instance, the co-crystallized ligands in 4BDS (Nachon et al., 2013) and 4B0O (Wandhammer et al., 2013) were retrieved with a RMSD of 0.37 and 1.65 \AA respectively. In agreement with the crystallized structure, the binding mode retrieved by the ligand tacrine in 4BDS located the heterocyclic scaffold near the residue Trp82 and established π - π stacking interactions with the residue. In the 4B0O structure, the pose described by docking retrieved the π - π stacking interactions between the benzylpyridinium group of the ligand and residues Trp82 and Tyr332. In addition, the trichloroacetimidate is oriented toward the same area in the receptor close to residues Thr120 and Ser287.

After docking simulations, all the compounds in our series yielded a similar binding mode that directed the triphenylphosphonium group toward the bottom of the pocket, close to the catalytic triad characterized by residues Ser198, Glu325 and His438, whereas the hydroxybenzamide was positioned toward the surface of the cavity (Figure 6). The most active compound in the series (AntiOxBEN₁) established a hydrogen bond between the nitrogen of the amide group and the residue Asn68. The binding mode also yielded additional hydrogen bonds with residues Asn68 and Glu276 by anchoring with the hydroxyl groups of the phenyl ring. Additionally, AntiOxBEN₁ established π - π stacking and π -cation interactions between the triphenylphosphonium group and residues Phe329 and Trp82. The residue Trp82 in the anionic site has been previously described as a key residue that establishes π -cation interactions with choline scaffolds (Nicolet et al., 2003; Bacalhau et al., 2016). A similar binding mode was detected for AntiOxBEN₂ with three hydroxyl groups in the phenyl ring. The introduction of a third hydroxyl group in the phenyl ring originated an additional hydrogen bond with the residue Asn289 (Figure 6). However, the hydroxyphenyl ring is slightly shifted toward the residue Asn289 causing the disruption of the hydrogen bond with residue Asn68. This fact could be related with the reduction of inhibitory activity shown by AntiOxBEN₂ in comparison to AntiOxBEN₁. Moreover, Coulomb interactions could play an important role in the ligand-protein recognition since there are different charged residues in the protein pocket and the studied compounds bear a positive charge in the phosphonium group. We calculated the Coulomb residue contributions to the binding for AntiOxBEN₁ and AntiOxBEN₂. The key contribution of some residues to the binding is represented in Figure 6D. Some residues showed important contributions, such as Glu276, Glu197, SBG198 (conjugated Ser in the aged enzyme), and Asp70. AntiOxBEN₁ and AntiOxBEN₂ presented some differences in the Coulomb energies for residues Glu276 and Asn289. While AntiOxBEN₂ showed a noticeable reduction of Coulomb interactions with residue Glu276 compared to AntiOxBEN₁, the interactions with the residue Asn289 were higher. The introduction of additional

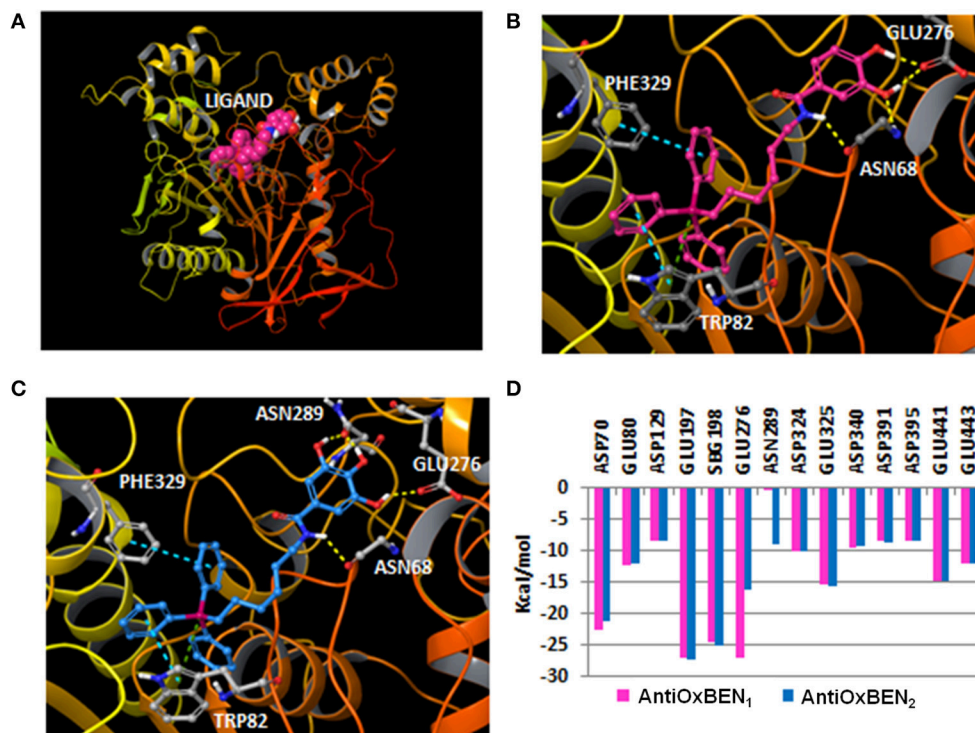


FIGURE 6 | (A) General perspective of **AntiOxBEN₁** (CPK representation) bound to the BChE (ribbons) extracted from molecular docking; **(B)** Binding mode calculated with molecular docking for **AntiOxBEN₁** (pink carbons) in the BChE (color code: yellow dashes for hydrogen bonds, blue dashes for π - π stacking interactions and green dashes for π -cation interactions); **(C)** Pose yielded by docking for **AntiOxBEN₂** (blue carbons) in the BChE; and **(D)** Coulomb residue contributions to the binding between the BChE and **AntiOxBEN₁** and **AntiOxBEN₂**.

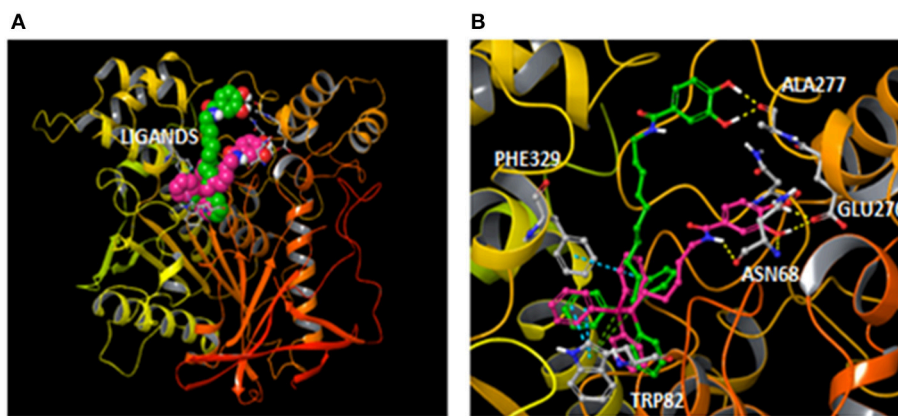


FIGURE 7 | (A) General overview with compounds **AntiOxBEN₁** and **17** (pink and green carbons respectively) bound to BChE after docking simulations; and **(B)** Comparison of the hypothetical binding modes determined for compounds **AntiOxBEN₁** (pink carbons) and **17** (green carbons) inside the BChE (color code: yellow dashes for hydrogen bonds, blue dashes for π - π stacking interactions and green dashes for π -cation interactions).

hydroxyl groups in the phenyl scaffold could be responsible for both the disruption and formation of ligand-protein interactions with a final decreased effect in the experimental activity. Moreover, the position of the third hydroxyl group is close to some hydrophobic residues, such as Leu286 and Val288 that define the acyl-binding pocket in the BChE. Polar substituents near this region could contribute to reduce the energy binding.

On the other hand, the enlargement of the aliphatic chain caused a slight reduction of the BChE activity. Molecular docking showed a binding mode for compound **17** with some differences regarding **AntiOxBEN₁**. Since compound **17** has an extended spacer length, the protein pocket accommodated the compound in a different binding position that could be responsible for the reduction of the activity. The hydroxybenzamide group was

accommodated in a shallower region of the protein pocket and established hydrogen bonds with the residue Ala277 (Figure 7). However, the different position of the hydroxybenzamide scaffold did not yield hydrogen bonds with residues Asn68 and Glu276 as AntiOxBEN₁. The proposed different binding mode for compound 17, due to the enlargement of the aliphatic chain between the triphenylphosphonium and the hydroxybenzamide groups, could be responsible for the reduction of BChE activity.

According to molecular modeling studies, this type of mitochondriotropic antioxidants are able to interact with both catalytic active site (CAS) and PAS of BChE and so they can act as bifunctional inhibitors (Brunhofer et al., 2012; Eckroat et al., 2013).

CONCLUSION

For the first time, dual target compounds based on mitochondriotropic antioxidants endowed with cholinesterase bifunctional inhibitory activity were described.

AntiOxBEN₁ acted as a selective and non-competitive BChE inhibitor and compounds 15–18 showed similar antioxidant and ChE inhibitory activities, when compared to AntiOxBEN₁ and AntiOxBEN₂. From the series, AntiOxBEN₁ and compound 18 were the most promising BChE and/or AChE inhibitors, respectively, acting by a non-competitive mechanism. Moreover, these compounds did not exhibit cytotoxic effects in both SH-SY5Y and HepG2 cells and significantly prevented A β _{1–42} peptide-induced dysfunction/cell death. Dual inhibition may also help to slow down the formation of amyloidogenic compounds, providing an important neuroprotective disease-modifying effect.

According to the BChE selectivity and antioxidant properties as well as drug-like properties, which points

toward BBB permeability, and favorable toxicological profile the mitochondriotropic antioxidant AntiOxBEN₁ is considered a valid candidate for the development of a dual acting drugs useful for AD therapy, which should be validated in animal models relevant for the disease.

AUTHOR CONTRIBUTIONS

CO: Synthesized the compounds, performed biological experiments, analyzed the data and wrote the paper; FC and LS: Helped in synthesis; JT and RA: Performed biological experiments, analyzed the data and refined the manuscript; FM, TS, JG, and FR: Helped in data analysis and also refined the manuscript; SV: Performed the molecular docking studies; EU, PO, and FB: Designed the project, experiments, and wrote the paper. All authors revised the manuscript and agreed with submission.

ACKNOWLEDGMENTS

This work was funded by FEDER funds through the Operational Programme Competitiveness Factors-COMPETE and national funds by FCT – Foundation for Science and Technology under research grants (QUI/UI0081/2013, NORTE-01-0145-FEDER-000028 and PTDC/DTP-FTO/2433/2014, POCI-01-0145-FEDER-016659, POCI-01-0145-FEDER-007440, CO (SFRH/BD/88773/2012), FC (SFRH/BPD/74491/2010), JT (PTDC/DTP-FTO/2433/2014 and NORTE-01-0145-FEDER-000028) RA (PTDC/DTP-FTO/2433/2014) grants are supported by FCT, POPH, and QREN. The authors also thank the COST action CA15135 for support.

REFERENCES

- Anand, P., and Singh, B. (2013). A review on cholinesterase inhibitors for Alzheimer's disease. *Arch. Pharm. Res.* 36, 375–399. doi: 10.1007/s12272-013-0036-3
- Apak, R., Capanoglu, E., and Shahidi, F. (2018). *Measurement of Antioxidant Activity and Capacity: Recent Trends and Applications*. Oxford, UK: Wiley.
- Bacalhau, P., San Juan, A. A., Goth, A., Caldeira, A. T., Martins, R., and Burke, A. J. (2016). Insights into (S)-rivastigmine inhibition of butyrylcholinesterase (BuChE): molecular docking and saturation transfer difference NMR (STD-NMR). *Bioorg. Chem.* 67, 105–109. doi: 10.1016/j.bioorg.2016.06.002
- Bajda, M., Wieckowska, A., Hebda, M., Guzior, N., Sotriffer, C. A., and Malawska, B. (2013). Structure-based search for new inhibitors of cholinesterases. *Int. J. Mol. Sci.* 14, 5608–5632. doi: 10.3390/ijms14035608
- Bhat, A. H., Dar, K. B., Anees, S., Zargar, M. A., Masood, A., Sofi, M. A., et al. (2015). Oxidative stress, mitochondrial dysfunction and neurodegenerative diseases; a mechanistic insight. *Biomed. Pharmacother.* 74, 101–110. doi: 10.1016/j.biopha.2015.07.025
- Brown, S. E., Ross, M. F., Sanjuan-Pla, A., Manas, A. R. B., Smith, R. A. J., and Murphy, M. P. (2007). Targeting lipoic acid to mitochondria: synthesis and characterization of a triphenylphosphonium-conjugated α -lipoyl derivative. *Free Radic. Biol. Med.* 42, 1766–1780. doi: 10.1016/j.freeradbiomed.2007.02.033
- Brunhofer, G., Fallarero, A., Karlsson, D., Batista-Gonzalez, A., Shinde, P., Gopi, M. C., et al. (2012). Exploration of natural compounds as sources of new bifunctional scaffolds targeting cholinesterases and beta amyloid aggregation: the case of chelerythrine. *Bioorg. Med. Chem.* 20, 6669–6679. doi: 10.1016/j.bmc.2012.09.040
- Chen, H., Xu, X., Liu, L., Tang, G., and Zhao, Y. (2013). Phosphorus oxychloride as an efficient coupling reagent for the synthesis of esters, amides and peptides under mild conditions. *RSC Adv.* 3, 16247–16250. doi: 10.1039/c3ra42887g
- Clark, D. E. (1999). Rapid calculation of polar molecular surface area and its application to the prediction of transport phenomena. 2. Prediction of blood-brain barrier penetration. *J. Pharm. Sci.* 88, 815–821. doi: 10.1021/js980402t
- Colović, M. B., Krstić, D. Z., Lazarević-Pašti, T. D., Bondžić, A. M., and Vasić, V. M. (2013). Acetylcholinesterase inhibitors: pharmacology and Toxicology. *Curr. Neuropharmacol.* 11, 315–335. doi: 10.2174/1570159X11311030006
- Dai, D. F., Chiao, Y. A., Marcinek, D. J., Szeto, H. H., and Rabinovitch, P. S. (2014). Mitochondrial oxidative stress in aging and healthspan. *Longev. Healthspan* 3:6. doi: 10.1186/2046-2395-3-6
- Dhawan, V. (2014). "Reactive oxygen and nitrogen species: general considerations," in *Studies on Respiratory Disorders*, eds N. K. Ganguly, S. K. Jindal, S. Biswal, P. J. Barnes, and R. Pawankar (New York, NY: Humana Press), 27–47.
- Di Giovanni, S., Borloz, A., Urbain, A., Marston, A., Hostettmann, K., Carrupt, P.-A., et al. (2008). *In vitro* screening assays to identify natural or synthetic acetylcholinesterase inhibitors: thin layer chromatography versus microplate methods. *Eur. J. Pharm. Sci.* 33, 109–119. doi: 10.1016/j.ejps.2007.10.004
- Eckroat, T. J., Green, K. D., Reed, R. A., Bornstein, J. J., and Garneau-Tsodikova, S. (2013). Investigation of the role of linker moieties in bifunctional tacrine hybrids. *Bioorg. Med. Chem.* 21, 3614–3623. doi: 10.1016/j.bmc.2013.02.047
- Ellman, G. L., Courtney, K. D., Andres, V., and Featherstone, R. M. (1961). A new and rapid colorimetric determination of acetylcholinesterase activity. *Biochem. Pharmacol.* 7, 88–95. doi: 10.1016/0006-2952(61)90145-9

- Fong, C. W. (2015). Permeability of the Blood-Brain Barrier: molecular mechanism of transport of drugs and physiologically important compounds. *J. Membr. Biol.* 248, 651–669. doi: 10.1007/s00232-015-9778-9
- Guo, C., Sun, L., Chen, X., and Zhang, D. (2013). Oxidative stress, mitochondrial damage and neurodegenerative diseases. *Neural Regen. Res.* 8, 2003–2014. doi: 10.3969/j.issn.1673-5374.2013.21.009
- Guzman-Villanueva, D., Mendiola, M., Nguyen, H., and Weissig, V. (2015). Influence of triphenylphosphonium (TPP) cation hydrophobization with phospholipids on cellular toxicity and mitochondrial selectivity. *SOJ Pharm. Pharm. Sci.* 2, 1–9. doi: 10.15226/2374-6866/2/1/00121
- Heleno, S. A., Martins, A., Queiroz, M. J., and Ferreira, I. C. (2015). Bioactivity of phenolic acids: metabolites versus parent compounds: a review. *Food. Chem.* 173, 501–513. doi: 10.1016/j.foodchem.2014.10.057
- Hitchcock, S. A., and Pennington, L. D. (2006). Structure brain exposure relationships. *J. Med. Chem.* 49, 7559–7583. doi: 10.1021/jm060642i
- Holmes, C., Ballard, C., Lehmann, D., David Smith, A., Beaumont, H., Day, I. N., et al. (2005). Rate of progression of cognitive decline in Alzheimer's disease: effect of butyrylcholinesterase K gene variation. *Neurol. Neurosurg. Psychiatry* 76, 640–643. doi: 10.1136/jnnp.2004.039321
- Ksiazek-Winiarek, D., and Głabinski, A. (2015). "The role of oxidative stress in neurodegenerative diseases," in *Studies on Psychiatric Disorders*, eds V. Dietrich-MuszalskaChauhan, and S. Grignon (New York, NY: Humana Press), 151–167.
- Li, Q., Yang, H., Chen, Y., and Sun, H. (2017). Recent progress in the identification of selective butyrylcholinesterase inhibitors for Alzheimer's disease. *Eur. J. Med. Chem.* 132, 294–309. doi: 10.1016/j.ejmech.2017.03.062
- Lin, Z., and Will, Y. (2012). Evaluation of drugs with specific organ toxicities in organ-specific cell lines. *Toxicol. Sci.* 126, 114–127. doi: 10.1093/toxsci/kfr339
- Lipinski, C. A., Lombardo, F., Dominy, B. W., and Feeney, P. J. (2001). Experimental and computational approaches to estimate solubility and permeability in drug discovery and development settings. *Adv. Drug. Deliv. Rev.* 46, 3–26. doi: 10.1016/S0169-409X(00)00129-0
- Lobner, D. (2000). Comparison of the LDH and MTT assays for quantifying cell death: validity for neuronal apoptosis? *J. Neurosci. Methods* 96, 147–152. doi: 10.1016/S0165-0270(99)00193-4
- Milhazes, N., Cunha-Oliveira, T., Martins, P., Garrido, J., Oliveira, C., Rego, A. C., et al. (2006). Synthesis and cytotoxic profile of 3,4-methylenedioxyamphetamin ("ecstasy") and its metabolites on undifferentiated PC12 cells: a putative structure-toxicity relationship. *Chem. Res. Toxicol.* 19, 1294–1304. doi: 10.1021/tx060123i
- Morán, M. A., Mufson, E. J., and Gómez-Ramos, P. (1993). Colocalization of cholinesterases with beta amyloid protein in aged and Alzheimer's brains. *Acta Neuropathol.* 85, 362–369. doi: 10.1007/BF00334445
- Murphy, M. P., and Smith, R. A. (2007). Targeting antioxidants to mitochondria by conjugation to lipophilic cations. *Annu. Rev. Pharmacol. Toxicol.* 47, 629–656. doi: 10.1146/annurev.pharmtox.47.120505.105110
- Nachon, F., Carletti, E., Ronco, C., Trovaslet, M., Nicolet, Y., Jean, L., et al. (2013). Crystal structures of human cholinesterases in complex with huprine W and tacrine: elements of specificity for anti-Alzheimer's drugs targeting acetyl- and butyryl-cholinesterase. *Biochem. J.* 453, 393–399. doi: 10.1042/BJ20130013
- Nicolet, Y., Lockridge, O., Masson, P., Fontecilla-Camps, J. C., and Nachon, F. (2003). Crystal structure of human butyrylcholinesterase and of its complexes with substrate and products. *J. Biol. Chem.* 278, 41141–41147. doi: 10.1074/jbc.M210241200
- Nikolic, K., Mavridis, L., Djikic, T., Vucicevic, J., Agbaba, D., Yelecki, K., et al. (2016). Drug design for CNS diseases: polypharmacological profiling of compounds using cheminformatic, 3D-QSAR and virtual screening methodologies. *Front. Neurosci.* 10:265. doi: 10.3389/fnins.2016.00265
- Pajouhesh, H., and Lenz, G. R. (2005). Medicinal chemical properties of successful central nervous system drugs. *NeuroRx* 2, 541–553. doi: 10.1602/neurorx.2.4.541
- Pezzini, I., Mattoli, V., and Ciofani, G. (2017). Mitochondria and neurodegenerative diseases: the promising role of nanotechnology in targeted drug delivery. *Expert Opin. Drug Deliv.* 14, 513–523. doi: 10.1080/17425247.2016.1218461
- Pohanka, M. (2014). Inhibitors of acetylcholinesterase and butyrylcholinesterase meet immunity. *Int. J. Mol. Sci.* 15, 9809–9825. doi: 10.3390/ijms15069809
- Pollastri, M. P., Sagal, J. F., and Chang, G. (2001). The conversion of alcohols to halides using a filterable phosphine source. *Tetrahedron Lett.* 42, 2459–2460. doi: 10.1016/S0040-4039(01)00220-9
- Rankovic, Z. (2015). CNS drug design: balancing physicochemical properties for optimal brain exposure. *J. Med. Chem.* 58, 2584–2608. doi: 10.1021/jm501535r
- Resende, R., Ferreiro, E., Pereira, C., and Oliveira, C. R. (2008). ER stress is involved in Abeta-induced GSK-3beta activation and tau phosphorylation. *J. Neurosci. Res.* 86, 2091–2099. doi: 10.1002/jnr.21648
- Schrödinger suite 2017-2 (2017). *Schrödinger Suite 2017-2*. Schrödinger, LLC and New York USA. Available online at: <http://www.schrodinger.com/> (Accessed: August 2017).
- Shah, A. A., Dar, T. A., Dar, P. A., Ganie, S. A., and Kamal, M. A. (2017). A current perspective on the inhibition of cholinesterase by natural and synthetic inhibitors. *Curr. Drug Metab.* 18, 96–111. doi: 10.2174/1389200218666161123122734
- Silva, F. S., Starostina, I. G., Ivanova, V. V., Rizvanov, A. A., Oliveira, P. J., and Pereira, S. P. (2016). Determination of metabolic viability and cell mass using a tandem resazurin/sulforhodamine B assay. *Curr. Protoc. Toxicol.* 68, 2.24.1–2.24.15. doi: 10.1002/cptx.1
- Silva, T., Reis, J., Teixeira, J., and Borges, F. (2014). Alzheimer's disease, enzyme targets and drug discovery struggles: from natural products to drug prototypes. *Ageing Res. Rev.* 15, 116–145. doi: 10.1016/j.arr.2014.03.008
- Sugimoto, H., Ogura, H., Arai, Y., Limura, Y., and Yamanishi, Y. (2002). Research and development of donepezil hydrochloride, a new type of acetylcholinesterase inhibitor. *Jpn. J. Pharmacol.* 89, 7–20. doi: 10.1254/jjp.89.7
- Szwajgier, D., Borowiec, K., and Pustelniak, K. (2017). The neuroprotective effects of phenolic acids: molecular mechanism of action. *Nutrients* 9:E477. doi: 10.3390/nu9050477
- Talevi, A. (2015). Multi-target pharmacology: possibilities and limitations of the "skeleton key approach" from a medicinal chemist perspective. *Front. Pharmacol.* 6:205. doi: 10.3389/fphar.2015.00205
- Teixeira, J., Cagide, F., Benfeito, S., Soares, P., Garrido, J., Baldeiras, I., et al. (2017a). Development of a mitochondriotropic antioxidant based on caffeic acid: proof of concept on cellular and mitochondrial oxidative stress models. *J. Med. Chem.* 60, 7084–7098. doi: 10.1021/acs.jmedchem.7b00741
- Teixeira, J., Oliveira, C., Amorim, R., Cagide, F., Garrido, J., Ribeiro, J. A., et al. (2017b). Development of hydroxybenzoic-based platforms as a solution to deliver dietary antioxidants to mitochondria. *Sci. Rep.* 7:6842. doi: 10.1038/s41598-017-07272-y
- Teixeira, J., Soares, P., Benfeito, S., Gaspar, A., Garrido, J., Murphy, M. P., et al. (2012). Rational discovery and development of a mitochondria-targeted antioxidant based on cinnamic acid scaffold. *Free Radic. Res.* 46, 600–611. doi: 10.3109/10715762.2012.662593
- Wandhammer, M., de Koning, M., van Grol, M., Loiodice, M., Saurel, L., Noort, D., et al. (2013). A step toward the reactivation of aged cholinesterases—crystal structure of ligands binding to aged human butyrylcholinesterase. *Chem. Biol. Interact.* 203, 19–23. doi: 10.1016/j.cbi.2012.08.005
- Zheng, H., Fridkin, M., and Youdim, M. (2014). From single target to multitarget/network therapeutics in Alzheimer's therapy. *Pharmaceuticals* 7, 113–135. doi: 10.3390/ph7020113.

Conflict of Interest Statement: PO and FB are co-founders of the start-up company MitoTAG. The other authors declare that the research was conducted in the absence of any commercial or financial relationships that could be construed as a potential conflict of interest.

The handling Editor declared a shared affiliation, though no other collaboration, with one of the authors, FM.

Copyright © 2018 Oliveira, Cagide, Teixeira, Amorim, Sequeira, Mesiti, Silva, Garrido, Remião, Vilar, Uriarte, Oliveira and Borges. This is an open-access article distributed under the terms of the Creative Commons Attribution License (CC BY). The use, distribution or reproduction in other forums is permitted, provided the original author(s) and the copyright owner are credited and that the original publication in this journal is cited, in accordance with accepted academic practice. No use, distribution or reproduction is permitted which does not comply with these terms.